The molecular mechanism and evolutionary divergence of caspase 3/7-regulated gasdermin E activation

Hang Xu[1,2,3], Zihao Yuan[1,2], Kunpeng Qin[1,2,3], Shuai Jiang[1,2,3*], Li Sun[1,2,3*]

[1]*CAS and Shandong Province Key Laboratory of Experimental Marine Biology, Institute of Oceanology; CAS Center for Ocean Mega-Science, Chinese Academy of Sciences, Qingdao, China*

[2]*Laboratory for Marine Biology and Biotechnology, Pilot National Laboratory for Marine Science and Technology, Qingdao, China*

[3]*University of Chinese Academy of Sciences, Beijing, China*

*To whom correspondence should be addressed

Email: sjiang@qdio.ac.cn; lsun@qdio.ac.cn

Abstract

Caspase (CASP) is a family of proteases involved in cleavage and activation of gasdermin, the executor of pyroptosis. In human, CASP3 and CASP7 recognize the same consensus motif DxxD, which is present in gasdermin E (GSDME). However, human GSDME is cleaved by CASP3 but not by CASP7. The underlying mechanism of this observation is unclear. In this study, we identified a pyroptotic pufferfish GSDME that was cleaved by both pufferfish CASP3/7 and human CASP3/7. Domain swapping between pufferfish and human CASP and GSDME showed that the GSDME C-terminus and the CASP7 p10 subunit determined the cleavability of GSDME by CASP7. p10 contains a key residue that governs CASP7 substrate discrimination. This key residue is highly conserved in vertebrate CASP3 and in most vertebrate (except mammalian) CASP7. In mammals, the key residue is conserved in non-primate (e.g., mouse) but not in primate. However, mouse CASP7 cleaved human GSDME but not mouse GSDME. These findings revealed the molecular mechanism of CASP7 substrate discrimination and the divergence of CASP3/7-mediated GSDME activation in vertebrate. These results also suggested that mutation-mediated functional alteration of CASP probably enabled the divergence and specialization of different CASP members in the regulation of complex cellular activities in mammals.

Key words

Immunity; Pyroptosis; Gasdermin E; Caspase 3; Caspase 7; Evolution

Introduction

Pyroptosis represents a form of programmed cell death that provokes robust inflammatory immune response (Bergsbaken, Fink, & Cookson, 2009; Tsuchiya et al., 2019). Gasdermin (GSDM) serves as the direct executioner of pyroptosis. GSDM forms transmembrane pores to permeabilize the cytoplasmic membrane, which leads to the release of pro-inflammatory cytokines and, if these transmembrane pores persist, pyroptosis (Kovacs & Miao, 2017; J. Shi, Gao, & Shao, 2017; Xia et al., 2021). Human has six GSDM (HsGSDM) family members, HsGSDMA-E，and HsPJVK (Tamura et al., 2007). All HsGSDMs (except for HsPJVK) adopt a two-domain architecture, the N-terminal (NT) pore-forming domain and the C-terminal (CT) autoinhibitory domain (De Schutter et al., 2021; Shao, 2021). Proteolytic cleavage of HsGSDM to remove the autoinhibitory CT domain enables the binding of the lipophilic NT fragment to the cell membrane, where the NT fragments oligomerize and form transmembrane pores to induce osmotic cell lysis (Kuang et al., 2017; X. Liu et al., 2016).

Among the signaling pathways that activate GSDM-mediated pyroptosis, caspase (CASP) 1/4/5/11-mediated GSDMD activation is well documented. In human, HsGSDMD is specifically cleaved by the inflammatory HsCASP1 through multiple inflammasome signaling pathways. HsCASP4/5 also cleave HsGSDMD in response to lipopolysaccharide (LPS) stimulation. After cleavage by HsCASP1/4/5, the pore-forming HsGSDMD-NT fragment becomes unconstrained and triggers pyroptosis (He et al., 2015; Kayagaki et al., 2015; J. Shi et al., 2015). Structural and biochemical analysis reveal that HsCASP1/4 βIII/βIII' sheet forms an exosite that interacts with the hydrophobic pocket of HsGSDMD-CT domain, rendering HsGSDMD cleavage independent of CASP recognition of the tetrapeptide motif FLTD (K. Wang et al., 2020). When the tetrapeptide FLTD is mutated to AAAD, HsCASP1/4 cleavage of HsGSDMD is not affected. The residues that form the hydrophobic pocket of HsGSDMD-CT domain are not conserved in HsGSDME, suggesting that HsGSDME cannot be cleaved by HsCASP1/4 via interaction with an exosite (Z. Liu et al., 2020).

Actually, human HsGSDME is specifically cleaved by HsCASP3 at the consensus motif DMPD, which is required for HsCASP3-mediated HsGSDME proteolysis. Mutation of either the Asp residue of the DMPD tetrapeptide motif leads to cleavage resistance of HsGSDME (Rogers et al., 2017; Wang et al., 2017), indicating that HsCASP3-mediated HsGSDME activation paradigm is distinct from that of HsGSDMD. It is intriguing that although HsCASP7 shares the same recognition motif (DxxD) with HsCASP3, HsCASP7 cannot cleave HsGSDME (Agniswamy, Fang, & Weber, 2009; Slee, Adrain, & Martin, 2001). The molecular mechanism underlying the HsCASP3/7 cleavage discrimination of HsGSDME is unknown.

Historically, HsCASP3 and HsCASP7, which are 54% identical, are known to possess similar structure and share overlapping protein substrate repertoire, and are considered to have functionally redundant roles in regulating cell death (Crawford & Wells, 2011; Kumar, 2007; Y. Shi, 2002). Both HsCASP3 and HsCASP7 consist of two polypeptide subunits named p20 and p10 (1:1 ratio), which assemble to form active heterotetramer (Timmer & Salvesen, 2007). HsCASP3/7 contain highly conserved QACRG and SHG motifs in p20 subunit, and SWR and GSWF motifs in p10 subunit, which participate in the catalytic reaction and substrate binding, respectively (Boyce, Degterev, & Yuan, 2004; Cohen, 1997). In the apoptosis signaling pathway, death receptor-mediated extrinsic pathway and mitochondria-mediated intrinsic pathway ultimately converge to the activation of HsCASP3/7 (Budd, Tenneti, Lishnak, & Lipton, 2000; Wajant, 2002). Active HsCASP3/7 cleave a series of protein substrates, including poly(ADP-ribose) polymerase and DNA fragmentation factor 45, which causes chromatin fragmentation and leads to apoptosis (Erener et al., 2012; Wolf, Schuler, Echeverri, & Green, 1999; Zheng et al., 1998). Although HsCASP3 and HsCASP7 exert almost indistinguishable proteolytic specificity to certain polypeptides, there exist functional differences between these two HsCASPs in cleaving some substrates (Brentnall, Rodriguez-Menocal, De Guevara, Cepero, & Boise, 2013; Demon et al., 2009). For instance, HsCASP3 cleaves Bid much more efficiently than HsCASP7, while HsCASP7 cleaves cochaperone p23 more efficiently than HsCASP3

(Slee et al., 2001; Walsh et al., 2008). These findings support the notion that HsCASP3 and HsCASP7 are enzymatically similar but functionally non-redundant.

Different from HsGSDME that is specifically cleaved by HsCASP3, teleost GSDME is cleaved via various modes (Angosto-Bazarra et al., 2022; Yuan, Jiang, Qin, & Sun, 2022). In this study, we identified a functional GSDME (named TrGSDME) from pufferfish *Takifugu rubripes*. We found that TrGSDME was specifically cleaved by both HsCASP3/7 and TrCASP3/7, whereas HsGSDME was cleaved by TrCASP3/7 and HsCASP3, but not by HsCASP7. We examined the underlying mechanism of this observation. We found that the GSDME-CT and the CASP7 p10 were critical for CASP7 cleavage of GSDME. By a series of site-directed mutagenesis, we discovered a previously unrecognized key residue (S234 in HsCASP7) in p10 that was responsible for the discriminative cleavage of HsGSDME by HsCASP7.

Results

Pufferfish GSDME is specifically cleaved by both human and fish CASP3/7

It has long been observed that although human caspase (HsCASP) 3 and 7 share the same consensus recognition motif DxxD, HsCASP3, but not HsCASP7, cleaves human GSDME (HsGSDME) (at the site of DMPD) (Poreba, Strozyk, Salvesen, & Drag, 2013; Wang et al., 2017). The underlying molecular mechanism is unknown. In this study, we found that a pufferfish *Takifugu rubripes* GSDME (designated TrGSDME), which belongs to the GSDMEa lineage of teleost GSDME (Figure-figure supplement 1), was specifically cleaved by both HsCASP3 and 7 (Figure 1A and B). This intriguing observation promoted us to explore the mechanism of HsCASP7 substrate discrimination. We first examined whether TrGSDME could be cleaved by pufferfish CASP (TrCASP) 3/7. The active forms of TrCASP3/7 were prepared (Figure 1C), both exhibited high proteolytic specificity and activity towards the tetrapeptide DEVD (Figure 1D and E), which is the conserved recognition motif of HsCASP3/7. When

incubated with TrGSDME, both TrCASP3 and TrCASP7 cleaved TrGSDME into the NT and CT fragments, similar to that cleaved by HsCASP3/7, in a dose dependent manner (Figure 1F and G). Accordingly, TrCASP3/7-mediated TrGSDME cleavage was inhibited by the CASP3 inhibitor (Z-DEVD-FMK) and the pan-CASP inhibitor (Z-VAD-FMK) (Figure 1H). Based on the molecular mass of the cleaved NT and CT products, we inferred that the tetrapeptide motif ^{255}DAVD^{258} in the vicinity of the linker region of TrGSDME may be the recognition site of CASP3/7. Indeed, the D255R and D258A mutants of TrGSDME were resistant to TrCASP3/7 and HsCASP3/7 cleavage (Figure 1I and J, Figure 1-figure supplement 2). Taken together, these results demonstrated that TrGSDME was cleaved by fish and human CASP3/7 in a manner that depended on the specific sequence of DAVD (Figure 1K).

CASP3/7-cleaved TrGSDME is functionally activated and induces pyroptosis.

We next examined whether TrGSDME, like HsGSDME, is a functional pyroptosis inducer. For this purpose, HEK293T cells were transfected with mCherry-tagged full length (FL) or NT/CT domain of TrGSDME. The results revealed that TrGSDME-FL and -CT were abundantly expressed in the cells, whereas TrGSDME-NT expression was barely detectable (Figure 2A, Figure 2-figure supplement 1). No significant morphological change or LDH release was observed in cells expressing TrGSDME-FL or -CT (Figure 2B and C). By contrast, cells expressing TrGSDME-NT showed necrotic cell death with massive LDH release and positive Sytox Green staining (Figure 2B and C, Figure 2-figure supplement 2). TrGSDME-NT-induced cell death exhibited osmotic cell membrane swelling, a typical feature of pyroptosis (Figure 2D). Time-lapse imaging showed that TrGSDME-NT triggered rapid cell swelling and membrane rupture, which led to release of cytoplasmic contents and eventually cell death (Figure 2E, Figure 1-video 1). To examine the pyroptotic activity of CASP3/7-cleaved TrGSDME, TrCASP3/7 and TrGSDME were overexpressed in HEK293T cells (Figure 2F and G). The cells expressing TrCASP3, TrCASP7 or TrGSDME alone had no apparent morphological change or LDH release, whereas the cells co-expressing

TrGSDME and TrCASP3 or TrGSDME and TrCASP7 underwent pyroptosis, accompanying with massive LDH release, membrane rupture, and TrGSDME cleavage (Figure 2G-I, Figure 2-figure supplement 3A). Consistently, the presence of the CASP3 inhibitor and pan-CASP inhibitor hampered TrGSDME-mediated pyroptosis (Figure 2J and K). Mutation of the cleavage site (D255R and D258A) inhibited pyroptosis and significantly decreased LDH release and TrGSDME cleavage (Figure 2L and M, Figure 2-figure supplement 3B and C). These results indicated that TrCASP3/7 cleavage was required to activate TrGSDME-mediated pyroptosis.

GSDME-CT domain mediates the recognition by CASP7.

Since it is known that human GSDME is cleaved by CASP3 but not by CASP7, the observation that TrGSDME was cleaved by both human and fish CASP3/7 intrigued us to explore the underlying mechanism. We found that unlike TrCASP1, both HsCASP3 and 7 exhibited proteolytic activity towards the consensus CASP3/7 recognition motif, DMPD, in HsGSDME, but HsCASP7 failed to cleave HsGSDME (Figure 3A and B, Figure 3-figure supplement 1 and 2). Structure analysis revealed that compared to TrGSDME, HsGSDME possesses two additional regions with the possibility to form a loop (261-266 aa) and an α-helix (281-296 aa), respectively (Figure 3C). We tested whether deletion of these two regions could confer HsCASP7 cleavage on HsGSDME. The results showed that similar to the wild type HsGSDME, the loop deletion mutant (Δ261-266) and the α-helix deletion mutant (Δ281-296) were cleaved by HsCASP3 but not by HsCASP7 (Figure 3D). Since the NT and CT domains play different roles in GSDM structure maintenance, we constructed GSDME chimeras consisting of HsGSDME-NT plus TrGSDME-CT (named HsNT-TrCT), or TrGSDME-NT plus HsGSDME-CT (named TrNT-HsCT) (Figure 3E). Compared with wild type HsGSDME and TrGSDME, chimeric HsNT-TrCT was cleaved by HsCASP3/7, whereas TrNT-HsCT was cleaved only by HsCASP3 (Figure 3F-I), suggesting that the CT domain determined the cleavability of GSDME by HsCASP7.

The p10 subunit determines the substrate specificity of CASP7.

Since as shown above, unlike HsCASP7, TrCASP7 was able to cleave HsGSDME (Figure 3H), we compared the sequences of TrCASP7 and HsCASP7. The two CASPs share 66.24% sequence identity. In these CASPs, the catalytic motifs SHG and QACRG in the p20 subunit and the substrate binding motifs SWR and GSWF in the p10 subunit are conserved (Figure 4A). To explore their substrate discrimination mechanism, we constructed CASP7 chimeras consisting of HsCASP7 p20 plus TrCASP7 p10 (named Hsp20-Trp10) or TrCASP7 p20 plus HsCASP7 p10 (named Trp20-Hsp10) (Figure 4B, Figure 4-figure supplement 1A). Compared to the wild types (HsCASP7 and TrCASP7), the chimeras exhibited comparable enzymatic activities towards the tetrapeptide substrates DAVD and DMPD (Figure 4C). Like the wild types, both chimeras cleaved TrGSDME and HsNT-TrCT (Figure 4D and E). By contrast, the Hsp20-Trp10 chimera cleaved HsGSDME, whereas the Trp20-Hsp10 chimera did not cleave HsGSDME (Figure 4F). Similar cleavage pattern was observed towards TrNT-HsCT (Figure 4G). These observations indicated that the p10 subunit dictated the cleavage specificity of CASP7 toward GSDME.

The S234 of p10 is the key to HsCASP7 discrimination on HsGSDME.

Comparative analysis of the p10 sequences of TrCASP7 and HsCASP7 identified 13 non-conserved residues. To examine their potential involvement in GSDME cleavage, a series of site-directed mutagenesis was performed to swap the non-conserved residues between HsCASP7 p10 and TrCASP7 p10 (Figure 5A, Figure 4-figure supplement 1B and C). Of the 13 swaps created, S234N conferred on HsCASP7 the ability to cleave HsGSDME (Figure 5B), whereas its corresponding swap in TrCASP7 (N245S) markedly reduced the ability of TrCASP7 to cleave HsGSDME (Figure 5C). None of the 13 swaps affected the ability of HsCASP7 or TrCASP7 to cleave TrGSDME (Figure 5D, E). HsCASP7-S234N cleaved HsGSDME in a dose-dependent manner (Figure 5F), and the cleavage was not enhanced by the additional mutation of S247N&I248V (Figure 5G). Additionally, HsCASP7 and HsCASP7-S234N exhibited similar cleavage

capacities against other CASP7 substrates, such as PARP1 and gelsolin (Figure 5-figure supplement 1) (Erener et al., 2012; Walsh et al., 2008). Previous studies showed that human CASP1/4 cleaved GSDMD through exosite interaction (Z. Liu et al., 2020; K. Wang et al., 2020). However, this exosite is not conserved in HsCASP7, in which the corresponding region forms a coil, not a β sheet (Figure 5-figure supplement 1). Structural modeling showed that the residues Q276, D278, and H283 are close to the region corresponding to the HsCASP1/4 exosite (Figure 5-figure supplement 1). Since these three residues are also not conserved between HsCASP7 p10 subunit and TrCASP7 p10 subunit, they were selected for mutagenesis to examine whether there existed an exosite interaction between HsCASP7 and HsGSDME. The mutation results showed that, similar to the wild type, the mutant Q276W&D278E&H283S was unable to cleave HsGSDME (Figure 5G), suggesting that, unlike human GSDMD, HsGSDME cleavage by CASPs probably did not involve exosite interaction. In contrast to HsGSDME, TrGSDME cleavage by HsCASP7 was not affected by the mutation of S234N, S234N plus S247N&I248V, or Q276W&D278E&H283S (Figure 5H).

All the above observed GSDME cleavages by CASP7 were verified in a cellular system. When co-expressed in HEK293T cells, HsGSDME was cleaved by TrCASP7 but not by HsCASP7, while TrGSDME was cleaved by both TrCASP7 and HsCASP7 (Figure 5-figure supplement 3). Additionally, both HsGSDME and TrGSDME were cleaved by HsCASP7-S234N as well as TrCASP7-N245S (Figure 5I and J). An apparent dose effect was observed in the cleavage of HsGSDME by HsCASP7-S234N (Figure 5K).

Divergent and GSDME-independent evolution of CASP7 leads to the loss of GSDME-activation function in mammalian CASP7.

Given the importance of N234 in p10 for HsCASP7 cleavage of HsGSDME, we analyzed the sequence conservation of this locus in CASP3/7. For CASP3, a highly conserved Asn residue (corresponding to HsCASP7 S234) was found immediately after the SWR motif in vertebrates (Figure 6A and B). In HsCASP3, this conserved Asn is

at position 208. We examined whether this residue was functionally essential to HsCASP3. Compared to the wild type, the N208S mutant exhibited much weaker cleavage of HsGSDME (Figure 6C, Figure 4-figure supplement 1D). Similar weakened cleavage was also observed in HEK293T cells co-expressing HsCASP3-N208S and HsGSDME (Figure 6D). These results indicated that the Asn residue was also critical for HsCASP3 cleavage of HsGSDME.

For CASP7, an Asn at the position corresponding to HsCASP7 S234 is highly conserved in teleost, amphibians, reptiles and birds, but not in mammals (Figure 6A). In mammals, the corresponding Asn is present in most non-primate species, such as mouse *Mus musculus* and bovine *Bos taurus*, but is replaced by Ser in primate, such as human *H. sapiens*, gorillas *Gorilla gorilla*, and chimpanzee *Pan troglodytes* (Figure 6E, Figure 6-figure supplement 1). We examined whether mouse CASP7 (MmCASP7) could cleave GSDME. The results showed that MmCASP7 cleaved HsGSDME in a dose-dependent manner, and the cleaving ability was abrogated by N234S mutation (Figure 6G and H, Figure 4-figure supplement 1E). By contrast, neither MmCASP7 nor MmCASP7-N234S was able to cleave mouse GSDME (MmGSDME) (Figure 6I). Mouse CASP3 (MmCASP3), however, cleaved MmGSDME efficiently (Figure 6-figure supplement 2). These results indicated the existence of an intra-species barrier for GSDME cleavage by CASP7 in some mammals, suggesting independent evolutions of CASP7 and GSDME.

Discussion

GSDME is an ancient member of the GSDM family existing ubiquitously in vertebrate from teleost to mammals (Broz, Pelegrin, & Shao, 2020; De Schutter et al., 2021). In human, GSDME is specifically cleaved by CASP3 at the consensus motif DMPD, but it is not cleaved by CASP7, which recognizes the same DxxD motif. CASP3 cleavage releases the pyroptosis-inducing NT fragment from the association of the inhibitory CT fragment and switches cell death from apoptosis to pyroptosis (Rogers et al., 2017; Wang et al., 2017). In this study, we found that different from human GSDME, a

pufferfish GSDME belonging to the teleost GSDMEa lineage was specifically cleaved by both CASP3 and CASP7 at the site of DAVD to liberate the pyroptosis-inducing NT fragment. In teleost, there generally exist two GSDME orthologs, named GSDMEa and GSDMEb. Comparative study on the functions of GSDMEa and GSDMEb is scarce, and it remains to be explored whether clear physiological roles are played by these two orthologs in fish. As executors of pyroptosis, teleost GSDMEs are activated via different mechanisms. In tongue sole *Cynoglossus semilaevis*, GSDMEb is preferably cleaved by CASP1 to trigger pyroptosis (Jiang, Gu, Zhao, & Sun, 2019); in zebrafish *Danio rerio*, GSDMEb is activated by caspy2 (CASP5 homolog) through the NLR family pyrin domain containing 3 (NLRP3) inflammasome signaling pathway (Li et al., 2020; Z. Wang et al., 2020). These observations indicate that similar to mammalian GSDMD, teleost GSDMEb is activated by inflammatory CASPs. In contrast, teleost GSDMEa is cleaved mainly by apoptotic CASPs. In zebrafish, GSDMEa is cleaved by CASP3 to generate the pyroptotic NT fragment (Wang et al., 2017). In turbot *Scophthalmus maximus*, GSDMEa is bi-directionally regulated by CASP3/7, which activate GSDMEa, and CASP6, which inactivates GSDMEa (Xu, Jiang, Yu, Yuan, & Sun, 2022). In common carp *Cyprinus carpio haematopterus*, GSDMEa is cleaved by CASP3 and induces pyroptosis (Zhao et al., 2022).The complicated scenario of GSDME-mediated pyroptosis signaling in fish is likely due to the reason that, unlike mammals that have multiple GSDM members to induce pyroptosis under different conditions, fish have only GSDME to induce pyroptotic cell death. Regulation by different CASPs may represent a mechanism that enables fish GSDME to execute the orders of different pyroptotic signals.

It is intriguing that, although HsCASP3 and 7 were indistinguishable in proteolysis towards the consensus tetrapeptide, they differed remarkably in the cleavage of HsGSDME and TrGSDME. HsCASP3, but not HsCASP7, cleaved HsGSDME, whereas both HsCASP3 and 7 cleaved TrGSDME at the same site. NT/CT domain swapping between HsGSDME and TrGSDME showed that chimeric GSDMEs containing the TrGSDME-CT domain were cleaved by human as well as pufferfish

CASP7 regardless of the source of the NT, whereas chimeric GSDMEs containing the HsGSDME-CT domain were resistant to HsCASP7. These results indicate that the CT domain, which is well accepted to exert an inhibitory effect on the pore-forming NT domain (Z. Liu et al., 2019; J. Shi et al., 2015), is the target of HsCASP7 discrimination, and hence determines the cleavability of GSDME by HsCASP7. Recently, Wang and Liu studied the molecular mechanism of human GSDMD recognition by CASP1/4, and showed that GSDMD-CT interacted with CASP1/4 exosites through binding to a hydrophobic pocket, which enhanced the recognition by CASP1/4 and contributed to tetrapeptide sequence-independent cleavage of GSDMD (Z. Liu et al., 2020; K. Wang et al., 2020). Different from GSDMD, we found that for TrGSDME, mutation of either the P4 (D255) or P1 (D258) residue of the consensus motif ^{255}DAVD^{258} made it resistant to CASP3/7, implying a lack of DAVD-independent cleavage mechanism. Similarly, a previous study observed that human and mouse GSDME harboring cleavage site (P4 or P1) mutation resisted CASP3 cleavage (Wang et al., 2017). These results suggest that, compared to GSDMD, GSDME has a distinct enzyme-substrate engagement mode that, as demonstrated in the present study, involves GSDME-CT.

Unlike HsCASP7, which was unable to cleave HsGSDME, TrCASP7 effectively cleaved HsGSDME. The swapping of p20 between HsCASP7 and TrCASP7 revealed that the two catalytic motifs in p20, i.e., SHG and QACRG, were not involved in HsCASP7 discrimination on GSDME. SWR and GSWF are known to be responsible for CASP substrate binding (Chai et al., 2001; Riedl et al., 2001). However, in our study, we found that these two motifs are conserved in human and pufferfish CASP7, and they had no apparent effect on the substrate discrimination of HsCASP7. By contrast, the chimeric HsCASP7 containing the p10 subunit of TrCASP7 acquired the ability to cleave HsGSDME, indicating an important role of p10. By a series of residue swapping and mutation analyses, we discovered that the residue in the position of 245 (in TrCASP7) or 234 (in HsCASP7) of the p10 subunit was the key that determined CASP7 cleavage of HsGSDME. Sequence analysis revealed that N245 is highly conserved in the CASP7 of teleost, amphibians, reptiles and birds. In contrast, this Asn

residue was changed to Ser in the CASP7 of mammals, especially primates, resulting in divergence of CASP7 from CASP3 in substrate recognition and cleavage. Since, unlike non-mammalian vertebrates, mammals possess multiple pyroptotic GSDM members (GSDMA, B, C, D, and E), the functional divergence of CASP7 from CASP3 may have occurred as a result of specific and non-redundant regulation of programmed cell death mediated by different executor molecules. One of the physiological consequences is that CASP7 frees itself from the GSDME-mediated pathway and thus is able to be engaged in other cellular processes. Another physiological consequence is that GSDME activation is limited to CASP3 cleavage, thus restricting GSDME activity to situations more specific, such as that inducing CASP3 activation. More physiological consequences of CASP3/7 divergence in GSDME activation need to be explored in future studies. With the exception of primates, the conserved Asn is present in a large number of mammals, including mice. Mouse CASP7 was able to cleave HsGSDME, further supporting the importance of the Asn in CASP7 recognition and cleavage. The inability of mouse CASP7 to cleave mouse GSDME is consistent with a previous report that CASP7 deletion had little effect on mouse GSDME-mediated pyroptosis (Sarhan et al., 2018). These results suggest mutually independent evolution of GSDME and CASP7 in mice, which likely has distanced GSDME and CASP7 from each other. Similarly, human CASP7 and GSDME may also have undergone independent evolution, which leads to the disengagement of GSDME from the substrate relationship with CASP7.

In conclusion, we identified a teleost GSDME that can be cleaved by fish and human CASP3/7 to trigger pyroptosis. The GSDME-CT domain and the CASP7 p10 subunit are critical in the determination of CASP7 cleavage of GSDME. Within the p10 subunit, a single residue plays a key role in CASP7 substrate recognition and cleavage. Our results reveal the molecular basis of the functional divergence of CASP7 and CASP3, and suggest separate evolutions of CASP7 and GSDME in mammals. These findings add new insights into CASP-regulated GSDME activation in lower and higher vertebrates.

Materials and Methods

Animal, ethics, and cell line

Clinically healthy pufferfish (*Takifugu rubripes*) were obtained from a local fish farm. In the laboratory, the fish were maintained at 19-20℃ in aerated seawater as reported previously (Xu et al., 2022). For euthanization, the fish were immersed in excess tricaine methane sulfonate (Sigma, St. Louis, MO). The animal experiments were approved by the Ethics Committee of institute of Oceanology, Chinese Academy of Sciences. HEK293T cells (ATCC, Rockville, MD, USA) were cultured in DMED medium (Corning, NY, USA) supplemented with 10% fetal bovine serum (ExCell Bio, Shanghai, China) at 37℃ in a 5% CO_2 incubator.

Sequence analysis

The sequences of 742 CASP3 and 758 CASP7 used in this study were downloaded from NCBI Orthologs. TrCASP7 and HsCASP7 sequences were aligned with Clustal W program (www.ebi.ac.uk/clustalw/) and visualized with ESPript 3.0 (http://espript.ibcp.fr/ESPript/cgi-bin/ESPript.cgi/) (Robert & Gouet, 2014). Conservation of S/N234 in CASP3/7 was analyzed via Weblogo3 (https://weblogo.threeplusone.com/) (Crooks, Hon, Chandonia, & Brenner, 2004), and the sequences of CASP3/7 used are shown in Table 1 and Table 2. The phylogenetic analysis of GSDME was performed as reported previously (Xu et al., 2022). The phylogenetic relationship of major mammalian clades was estimated based on the Mammals birth-death node-dated completed trees in VertLife (Upham, Esselstyn, & Jetz, 2019). The phylogenetic tree was subsequently viewed and edited in iTOL (Letunic & Bork, 2021). The icons representing phylogeny clades were retrieved from the PhyloPic (http://www.phylopic.org/), with the detailed credentials provided in Table 3.

Antibodies and immunoblotting

Monoclonal anti-mouse (ab215191) and anti-human (ab221843) GSDME antibodies were purchased from Abcam (Cambridge, MA). Antibodies against β-actin (AC026), Flag (AE005), Myc (AE010), His (AE003), and mCherry (AE002) were purchased from Abclonal (Wuhang, China). Mouse polyclonal antibody against TrGSDME was prepared as reported previously (Xu et al., 2022). Anti-serum (1:1000 dilution) was used for immunoblotting. Immunoblotting was performed as reported previously (Zhao & Sun, 2022). Briefly, the samples were fractionated in 12% SDS-polyacrylamide gels (GenScript, Piscataway, NJ, USA). The proteins were transferred to NC membranes, immunobloted with appropriate antibodies and visualized using an ECL kit (Sparkjade Biotechnology Co. Ltd., Shandong, China).

Gene cloning and mutagenesis

Total RNA was extracted from pufferfish kidney using the FastPure Cell/Tissue Total RNA Isolation Kit V2 (Vazyme Biotech Co. Ltd., Nanjing, China). cDNA synthesis was performed with Revert Aid First Strand cDNA Synthesis Kit (Thermo Fisher Scientific, Waltham, MA, United States). The coding sequences (CDSs) of pufferfish GSDME (Accession number XP_029701077.1) and CASP3/7 were amplified by PCR. The CDSs of mouse GSDME and CASP3/7 were synthesized by Sangon Biotech (Shanghai, China). Site-directed mutagenesis was performed using Hieff Mut Site-Directed Mutagenesis Kit (Yeasen, Shanghai, China). Truncates of TrGSDME were created as reported previously (Xu et al., 2022) and subcloned into pmCherry-N1 (Clontech, Mountain View, CA, USA). For the construction of GSDME and CASP7 chimera, the CDSs of GSDME NT/CT and CASP7 p10/p20 were obtained by PCR and ligated. The constructs of the truncate and chimeric proteins are shown in Table 4. All sequences/constructs were verified by sequencing analysis. The primers used are listed in Table 5.

Plasmids and transient expression

For expression in mammalian cell expression, the CDSs of GSDME (pufferfish, human and mouse) were subcloned into pCS2-3×Flag (Wang et al., 2017) or pmCherry-N1 and CDSs encoding CASP (pufferfish, human and mouse) were subcloned into p-CMV-Myc (Clontech, Mountain View, CA, USA) or pCS2-Myc (Wang et al., 2017). All plasmids were prepared with endotoxin-free plasmid kit (Sparkjade Biotechnology Co. Ltd., Shandong, China). For transient expression, HEK293T cells were cultured in 96- or 24-well plates (Corning, NY, USA) overnight, and then transfected with 100 ng/well (96-well plates) or 500 ng/well (24-well plates) indicated plasmids using Liopfectamine 3000 (Invitrogen, USA) for 24 h or as specified. For GSDME processing, the plasmids of GSDME and CASP were co-transfected in HEK293T cells as described above and cultured continuously for 24 h or as specified. Cells were harvested and lysed with RIPA Lysis Buffer (Beyotime, Shanghai, China) for immunoblotting. The primer used are shown in Table 5.

Protein purification

Recombinant GSDMEs and CASPs are all soluble and were purified as described previously (Jiang, Zhou, Sun, Zhang, & Sun, 2020; Xu et al., 2022). Briefly, the CDSs of TrGSDME and CASP variants were each cloned into pET30a (+), and the CDSs of HsGSDME, MmGSDME, and chimeric GSDME were each cloned into pET28a-SUMO. The recombinant plasmids were introduced into *Escherichia coli* Transetta (DE3) (TransGen, Beijing, China) by transformation. The transformants were cultured in Luria broth (LB) at 37℃ until logarithmic growth phase. Isopropyl-β-D-thiogalactopyranoside (0.3 mM) was added to the medium, followed by incubation at 16℃ for 20 h. Bacteria were harvested and lysed, and the supernatant was collected for protein purification with Ni-NTA columns (GE Healthcare, Uppsala, Sweden). The proteins were dialyzed with PBS at 4 °C and concentrated.

CASP activity

To measure their proteolytic activity, recombinant CASPs were incubated separately with various colorimetric substrates at 37℃ for 2 h as described previously (Jiang et al., 2020; Xu et al., 2022), and then monitored for released ρNA at OD405. To compare their substrate preference, TrCASP3/7 and HsCASP3/7 were incubated with Ac-DAVD-ρNA or Ac-DMPD-ρNA (Science Peptide Biological Technology Co., Ltd, shanghai, China) at 37℃ for 30 min, and the released ρNA was measured at OD405. The CASP activity in cells transfected TrCASP3/7 was determined as described previously (Xu et al., 2022).

GSDME cleavage by CASPs

GSDME cleavage assay was performed as described previously (Jiang et al., 2020; Xu et al., 2022). Briefly, recombinant GSDME was incubated with 1 U of recombinant HsCASP1 ,2, 3, 6, 7, 8 and 9 (Enzo Life Sciences, Villeurbanne, France) at 37℃ for 2 h in the reaction buffer (50 mM Hepes (pH 7.5), 3 mM EDTA, 150 mM NaCl, 0.005% (v/v) Tween 20, and 10 mM DTT). TrGSDME, HsGSDME or their chimeras were treated with 1 U of TrCASP3/7, HsCASP3/7, or their chimeras for 2 h as above in reaction buffer. After incubation, the samples were boiled in 5 x Loading Buffer (GenScript, Piscataway, NJ, USA) and subjected to SDS-PAGE or immunoblotting with indicated antibody.

Cell death examination

Cell death examination by microscopy was performed as reported previously (Jiang et al., 2020; Xu et al., 2022). Briefly, HEK293T cells were plated into 35 mm glass-bottom culture dishes (Nest Biotechnology, Wuxi, China) at about 60% confluency and subjected to the indicated treatment for 24 h. To examine cell death morphology, propidium iodide (PI) (Invitrogen, Carlsbad, CA, USA) and DiO (Solarbio, Beijing, China) were added to the culture medium, and the cells were observed with a Carl Zeiss LSM 710 confocal microscope (Carl Zeiss, Jena, Germany). To video the cell death process, the cells were transfected with 1 μg pmCherry-N1 vector expressing

TrGSDME-NT for 16 h, and cell death was recorded using the above microscope. Cell death measured by lactate dehydrogenase (LDH) assay was performed as reported previously (Xu et al., 2022).

Statistical analysis

The Student's t test and one-way analysis of variance (ANOVA) were used for comparisons between groups. Statistical analysis was performed with GraphPad Prism 7 software. Statistical significance was defined as $P < 0.05$.

Acknowledgments

We thank Prof. Feng Shao (National institute of Biological Sciences, Beijing, China) for providing human CASP3/7 and GSDME expression vectors. This work was supported by the grants from the Science & Technology Innovation Project of Laoshan Laboratory (LSKJ202203000), the Youth Innovation Promotion Association CAS (2021204), the National Natural Science Foundation of China (41876175), and the Taishan Scholar Program of Shandong Province (2018 and 2021).

Author Contributions

Hang Xu: Methodology; Investigation; Visualization; Writing—original draft. ;**Zihao Yuan**: Investigation. **Kunpeng Qin**: Investigation; **Shuai Jiang**: Conceptualization; Methodology; Supervision; Writing—review & editing. **Li Sun**: Conceptualization; Supervision; Writing—review & editing.

Competing Interest Statement

The authors declare that they have no competing interests.

References

Agniswamy, J., Fang, B., & Weber, I. T. (2009). Conformational similarity in the activation of caspase-3 and -7 revealed by the unliganded and inhibited structures of caspase-7. *Apoptosis, 14*(10), 1135-1144. doi:10.1007/s10495-009-0388-9

Angosto-Bazarra, D., Alarcon-Vila, C., Hurtado-Navarro, L., Banos, M. C., Rivers-Auty, J., & Pelegrin, P. (2022). Evolutionary analyses of the gasdermin family suggest conserved roles in infection response despite loss of pore-forming functionality. *BMC Biol, 20*(1), 9. doi:10.1186/s12915-021-01220-z

Bergsbaken, T., Fink, S. L., & Cookson, B. T. (2009). Pyroptosis: host cell death and inflammation. *Nat Rev Microbiol, 7*(2), 99-109. doi:10.1038/nrmicro2070

Boyce, M., Degterev, A., & Yuan, J. (2004). Caspases: an ancient cellular sword of Damocles. *Cell Death Differ, 11*(1), 29-37. doi:10.1038/sj.cdd.4401339

Brentnall, M., Rodriguez-Menocal, L., De Guevara, R. L., Cepero, E., & Boise, L. H. (2013). Caspase-9, caspase-3 and caspase-7 have distinct roles during intrinsic apoptosis. *BMC Cell Biol, 14*, 32. doi:10.1186/1471-2121-14-32

Broz, P., Pelegrin, P., & Shao, F. (2020). The gasdermins, a protein family executing cell death and inflammation. *Nat Rev Immunol, 20*(3), 143-157. doi:10.1038/s41577-019-0228-2

Budd, S. L., Tenneti, L., Lishnak, T., & Lipton, S. A. (2000). Mitochondrial and extramitochondrial apoptotic signaling pathways in cerebrocortical neurons. *Proc Natl Acad Sci U S A, 97*(11), 6161-6166. doi:10.1073/pnas.100121097

Chai, J., Shiozaki, E., Srinivasula, S. M., Wu, Q., Datta, P., Alnemri, E. S., & Shi, Y. (2001). Structural basis of caspase-7 inhibition by XIAP. *Cell, 104*(5), 769-780. doi:10.1016/s0092-8674(01)00272-0

Cohen, G. M. (1997). Caspases: the executioners of apoptosis. *Biochem J, 326 (Pt 1)*, 1-16. doi:10.1042/bj3260001

524 Crawford, E. D., & Wells, J. A. (2011). Caspase substrates and cellular remodeling.
525 *Annu Rev Biochem, 80*, 1055-1087. doi:10.1146/annurev-biochem-061809-
526 121639
527 Crooks, G. E., Hon, G., Chandonia, J. M., & Brenner, S. E. (2004). WebLogo: a
528 sequence logo generator. *Genome Res, 14*(6), 1188-1190. doi:10.1101/gr.849004
529 De Schutter, E., Roelandt, R., Riquet, F. B., Van Camp, G., Wullaert, A., &
530 Vandenabeele, P. (2021). Punching Holes in Cellular Membranes: Biology and
531 Evolution of Gasdermins. *Trends Cell Biol, 31*(6), 500-513.
532 doi:10.1016/j.tcb.2021.03.004
533 Demon, D., Van Damme, P., Vanden Berghe, T., Deceuninck, A., Van Durme, J.,
534 Verspurten, J., . . . Vandenabeele, P. (2009). Proteome-wide substrate analysis
535 indicates substrate exclusion as a mechanism to generate caspase-7 versus
536 caspase-3 specificity. *Mol Cell Proteomics, 8*(12), 2700-2714.
537 doi:10.1074/mcp.M900310-MCP200
538 Erener, S., Petrilli, V., Kassner, I., Minotti, R., Castillo, R., Santoro, R., . . . Hottiger,
539 M. O. (2012). Inflammasome-activated caspase 7 cleaves PARP1 to enhance the
540 expression of a subset of NF-kappaB target genes. *Mol Cell, 46*(2), 200-211.
541 doi:10.1016/j.molcel.2012.02.016
542 He, W. T., Wan, H., Hu, L., Chen, P., Wang, X., Huang, Z., . . . Han, J. (2015).
543 Gasdermin D is an executor of pyroptosis and required for interleukin-1beta
544 secretion. *Cell Res, 25*(12), 1285-1298. doi:10.1038/cr.2015.139
545 Jiang, S., Gu, H., Zhao, Y., & Sun, L. (2019). Teleost Gasdermin E Is Cleaved by
546 Caspase 1, 3, and 7 and Induces Pyroptosis. *J Immunol, 203*(5), 1369-1382.
547 doi:10.4049/jimmunol.1900383
548 Jiang, S., Zhou, Z., Sun, Y., Zhang, T., & Sun, L. (2020). Coral gasdermin triggers
549 pyroptosis. *Sci Immunol, 5*(54). doi:10.1126/sciimmunol.abd2591
550 Kayagaki, N., Stowe, I. B., Lee, B. L., O'Rourke, K., Anderson, K., Warming, S., . . .
551 Dixit, V. M. (2015). Caspase-11 cleaves gasdermin D for non-canonical
552 inflammasome signalling. *Nature, 526*(7575), 666-671. doi:10.1038/nature15541

553 Kovacs, S. B., & Miao, E. A. (2017). Gasdermins: Effectors of Pyroptosis. *Trends Cell*
554 *Biol, 27*(9), 673-684. doi:10.1016/j.tcb.2017.05.005
555 Kuang, S., Zheng, J., Yang, H., Li, S., Duan, S., Shen, Y., . . . Li, J. (2017). Structure
556 insight of GSDMD reveals the basis of GSDMD autoinhibition in cell pyroptosis.
557 *Proc Natl Acad Sci U S A, 114*(40), 10642-10647. doi:10.1073/pnas.1708194114
558 Kumar, S. (2007). Caspase function in programmed cell death. *Cell Death Differ, 14*(1),
559 32-43. doi:10.1038/sj.cdd.4402060
560 Letunic, I., & Bork, P. (2021). Interactive Tree Of Life (iTOL) v5: an online tool for
561 phylogenetic tree display and annotation. *Nucleic Acids Res, 49*(W1), W293-
562 W296. doi:10.1093/nar/gkab301
563 Li, J. Y., Wang, Y. Y., Shao, T., Fan, D. D., Lin, A. F., Xiang, L. X., & Shao, J. Z.
564 (2020). The zebrafish NLRP3 inflammasome has functional roles in ASC-
565 dependent interleukin-1beta maturation and gasdermin E-mediated pyroptosis. *J*
566 *Biol Chem, 295*(4), 1120-1141. doi:10.1074/jbc.RA119.011751
567 Liu, X., Zhang, Z., Ruan, J., Pan, Y., Magupalli, V. G., Wu, H., & Lieberman, J. (2016).
568 Inflammasome-activated gasdermin D causes pyroptosis by forming membrane
569 pores. *Nature, 535*(7610), 153-158. doi:10.1038/nature18629
570 Liu, Z., Wang, C., Yang, J., Chen, Y., Zhou, B., Abbott, D. W., & Xiao, T. S. (2020).
571 Caspase-1 Engages Full-Length Gasdermin D through Two Distinct Interfaces
572 That Mediate Caspase Recruitment and Substrate Cleavage. *Immunity, 53*(1), 106-
573 114 e105. doi:10.1016/j.immuni.2020.06.007
574 Liu, Z., Wang, C., Yang, J., Zhou, B., Yang, R., Ramachandran, R., . . . Xiao, T. S.
575 (2019). Crystal Structures of the Full-Length Murine and Human Gasdermin D
576 Reveal Mechanisms of Autoinhibition, Lipid Binding, and Oligomerization.
577 *Immunity, 51*(1), 43-49 e44. doi:10.1016/j.immuni.2019.04.017
578 Poreba, M., Strozyk, A., Salvesen, G. S., & Drag, M. (2013). Caspase Substrates and
579 Inhibitors. *Cold Spring Harbor Perspectives in Biology, 5*(8), a008680-a008680.
580 doi:10.1101/cshperspect.a008680

581 Riedl, S. J., Renatus, M., Schwarzenbacher, R., Zhou, Q., Sun, C., Fesik, S. W., . . .
582 Salvesen, G. S. (2001). Structural basis for the inhibition of caspase-3 by XIAP.
583 *Cell, 104*(5), 791-800. doi:10.1016/s0092-8674(01)00274-4
584 Robert, X., & Gouet, P. (2014). Deciphering key features in protein structures with the
585 new ENDscript server. *Nucleic Acids Res, 42*(Web Server issue), W320-324.
586 doi:10.1093/nar/gku316
587 Rogers, C., Fernandes-Alnemri, T., Mayes, L., Alnemri, D., Cingolani, G., & Alnemri,
588 E. S. (2017). Cleavage of DFNA5 by caspase-3 during apoptosis mediates
589 progression to secondary necrotic/pyroptotic cell death. *Nat Commun, 8*, 14128.
590 doi:10.1038/ncomms14128
591 Sarhan, J., Liu, B. C., Muendlein, H. I., Li, P., Nilson, R., Tang, A. Y., . . . Poltorak, A.
592 (2018). Caspase-8 induces cleavage of gasdermin D to elicit pyroptosis during
593 Yersinia infection. *Proc Natl Acad Sci U S A, 115*(46), E10888-E10897.
594 doi:10.1073/pnas.1809548115
595 Shao, F. (2021). Gasdermins: making pores for pyroptosis. *Nat Rev Immunol, 21*(10),
596 620-621. doi:10.1038/s41577-021-00602-2
597 Shi, J., Gao, W., & Shao, F. (2017). Pyroptosis: Gasdermin-Mediated Programmed
598 Necrotic Cell Death. *Trends Biochem Sci, 42*(4), 245-254.
599 doi:10.1016/j.tibs.2016.10.004
600 Shi, J., Zhao, Y., Wang, K., Shi, X., Wang, Y., Huang, H., . . . Shao, F. (2015). Cleavage
601 of GSDMD by inflammatory caspases determines pyroptotic cell death. *Nature,*
602 *526*(7575), 660-665. doi:10.1038/nature15514
603 Shi, Y. (2002). Mechanisms of caspase activation and inhibition during apoptosis. *Mol*
604 *Cell, 9*(3), 459-470. doi:10.1016/s1097-2765(02)00482-3
605 Slee, E. A., Adrain, C., & Martin, S. J. (2001). Executioner caspase-3, -6, and -7
606 perform distinct, non-redundant roles during the demolition phase of apoptosis. *J*
607 *Biol Chem, 276*(10), 7320-7326. doi:10.1074/jbc.M008363200
608 Tamura, M., Tanaka, S., Fujii, T., Aoki, A., Komiyama, H., Ezawa, K., . . . Shiroishi,
609 T. (2007). Members of a novel gene family, Gsdm, are expressed exclusively in

610 the epithelium of the skin and gastrointestinal tract in a highly tissue-specific
611 manner. *Genomics, 89*(5), 618-629. doi:10.1016/j.ygeno.2007.01.003
612 Timmer, J. C., & Salvesen, G. S. (2007). Caspase substrates. *Cell Death Differ, 14*(1),
613 66-72. doi:10.1038/sj.cdd.4402059
614 Tsuchiya, K., Nakajima, S., Hosojima, S., Thi Nguyen, D., Hattori, T., Manh Le, T., . . .
615 Suda, T. (2019). Caspase-1 initiates apoptosis in the absence of gasdermin D. *Nat*
616 *Commun, 10*(1), 2091. doi:10.1038/s41467-019-09753-2
617 Upham, N. S., Esselstyn, J. A., & Jetz, W. (2019). Inferring the mammal tree: Species-
618 level sets of phylogenies for questions in ecology, evolution, and conservation.
619 *PLoS Biol, 17*(12), e3000494. doi:10.1371/journal.pbio.3000494
620 Wajant, H. (2002). The Fas signaling pathway: more than a paradigm. *Science,*
621 *296*(5573), 1635-1636. doi:10.1126/science.1071553
622 Walsh, J. G., Cullen, S. P., Sheridan, C., Luthi, A. U., Gerner, C., & Martin, S. J. (2008).
623 Executioner caspase-3 and caspase-7 are functionally distinct proteases. *Proc Natl*
624 *Acad Sci U S A, 105*(35), 12815-12819. doi:10.1073/pnas.0707715105
625 Wang, K., Sun, Q., Zhong, X., Zeng, M., Zeng, H., Shi, X., . . . Ding, J. (2020).
626 Structural Mechanism for GSDMD Targeting by Autoprocessed Caspases in
627 Pyroptosis. *Cell, 180*(5), 941-955 e920. doi:10.1016/j.cell.2020.02.002
628 Wang, Y., Gao, W., Shi, X., Ding, J., Liu, W., He, H., . . . Shao, F. (2017).
629 Chemotherapy drugs induce pyroptosis through caspase-3 cleavage of a gasdermin.
630 *Nature, 547*(7661), 99-103. doi:10.1038/nature22393
631 Wang, Z., Gu, Z., Hou, Q., Chen, W., Mu, D., Zhang, Y., . . . Yang, D. (2020). Zebrafish
632 GSDMEb Cleavage-Gated Pyroptosis Drives Septic Acute Kidney Injury In Vivo.
633 *J Immunol, 204*(7), 1929-1942. doi:10.4049/jimmunol.1901456
634 Wolf, B. B., Schuler, M., Echeverri, F., & Green, D. R. (1999). Caspase-3 is the primary
635 activator of apoptotic DNA fragmentation via DNA fragmentation factor-
636 45/inhibitor of caspase-activated DNase inactivation. *J Biol Chem, 274*(43),
637 30651-30656. doi:10.1074/jbc.274.43.30651

638 Xia, S., Zhang, Z., Magupalli, V. G., Pablo, J. L., Dong, Y., Vora, S. M., . . . Wu, H.
639 (2021). Gasdermin D pore structure reveals preferential release of mature
640 interleukin-1. *Nature*. doi:10.1038/s41586-021-03478-3
641 Xu, H., Jiang, S., Yu, C., Yuan, Z., & Sun, L. (2022). GSDMEa-mediated pyroptosis is
642 bi-directionally regulated by caspase and required for effective bacterial clearance
643 in teleost. *Cell Death Dis, 13*(5), 491. doi:10.1038/s41419-022-04896-5
644 Yuan, Z., Jiang, S., Qin, K., & Sun, L. (2022). New insights into the evolutionary
645 dynamic and lineage divergence of gasdermin E in metazoa. *Front Cell Dev Biol,*
646 *10*, 952015. doi:10.3389/fcell.2022.952015
647 Zhao, Y., & Sun, L. (2022). Bacillus cereus cytotoxin K triggers gasdermin D-
648 dependent pyroptosis. *Cell Death Discov, 8*(1), 305. doi:10.1038/s41420-022-
649 01091-5
650 Zhao, Y., Zhang, J., Qiao, D., Gao, F., Gu, Y., Jiang, X., . . . Kong, X. (2022).
651 CcGSDMEa functions the pore-formation in cytomembrane and the regulation on
652 the secretion of IL-lbeta in common carp (Cyprinus carpio haematopterus). *Front*
653 *Immunol, 13*, 1110322. doi:10.3389/fimmu.2022.1110322
654 Zheng, T. S., Schlosser, S. F., Dao, T., Hingorani, R., Crispe, I. N., Boyer, J. L., &
655 Flavell, R. A. (1998). Caspase-3 controls both cytoplasmic and nuclear events
656 associated with Fas-mediated apoptosis in vivo. *Proc Natl Acad Sci U S A, 95*(23),
657 13618-13623. doi:10.1073/pnas.95.23.13618

658

659

Figure legends

Figure 1. Cleavage of TrGSDME by caspases. (A, B) TrGSDME was treated with 1 U of different HsCASPs for 2 h and then subjected to SDS-PAGE (A) and immunoblotting (B). **(C)** SDS-PAGE analysis of purified TrCASP3/7. The p10 and p20 subunits are indicated. **(D)** TrCASP3/7 cleavage of different colorimetric CASP substrates was monitored by measuring released ρNA. The values are the means ± SD of three replicates. **(E)** TrCASP3/7 (0.25-8U) were incubated with Ac-DEVD-ρNA, and time-dependent release of ρNA was measured. **(F, G)** SDS-PAGE (F) and immunoblotting (G) analysis of TrGSDME cleavage by TrCASP3/7 (0.25-4U). **(H)** TrGSDME cleavage by TrCASP3/7 was determined in the presence or absence of 20 μM Z-DEVD-FMK or Z-VAD-FMK. **(I, J)** TrGSDME wild type (WT) and mutants (D255R or D258A) were incubated with TrCASP3/7 for 2 h, and the cleavage was determined by SDS-PAGE (I) and immunoblotting (J). **(K)** A schematic of TrGSDME cleavage by TrCASP3/7. The arrow indicates cleavage site. For all panels, FL, full length; NT, N-terminal fragment; CT, C-terminal fragment.

Figure 2. The pyroptotic activity of TrGSDME. (A-C) HEK293T cells were transfected with C-terminally mCherry-tagged TrGSDME full length (FL) or truncate (NT or CT) for 24 h, and then analyzed for TrGSDME expression (A), morphological change (B), and LDH release (C). Scale bars, 50 μm (A) and 20 μm (B). **(D)** HEK293T cells were transfected with the backbone vector or vector expressing Myc-tagged TrGSDME-NT for 24 h. The cell nuclei and membrane were stained with PI and DiO, respectively. Scale bar, 10 μm. **(E)** HEK293T cells were transfected with mCherry-tagged TrGSDME-NT for 16 h, and the progression of cell death was shown by time-lapse microscopic imaging. Scale bar, 10 μm. **(F)** HEK293T cells were transfected with TrCASP3/7 for 24 h, and the proteolytic activity of TrCASP3/7 was assessed by treatment with fluorogenic Ac-DEVD-AFC. **(G)** Phase-contrast images of HEK293T cells transfected with the indicated vectors for 24 h. Scale bar, 20 μm. **(H, I)** LDH release (H) and TrGSDME cleavage and TrCASP3/7 expression (I) in the above

transfected cells were determined. For panel (I), FL, full-length; CT, C-terminal fragment. **(J, K)** HEK293T cells co-expressing TrGSDME and TrCASP3/7 for 24 h in the presence or absence (control) of 10 μM Z-VAD-FMK or Z-DEVD-FMK were subjected to microscopy (J) and LDH measurement (K). Scale bar, 20 μm. **(L, M)** HEK293T cells expressing TrCASP3/7 plus TrGSDME or TrCASP3/7 plus the D255R/D258A mutant were subjected to microscopy (L) and LDH measurement (M). Scale bar, 20 μm. For panels (C, F, H, K and M), values are the means of three experimental replicates and shown as means ± SD. $^{**}P < 0.01$, $^{***}P < 0.001$.

Figure 3. GSDME-CT domain determines the recognition by CASP7. (A) HsGSDME was treated with 1 U of various HsCASPs for 2 h, and the products were analyzed by immunoblotting with anti-HsGSDME-CT antibody. **(B)** HsCASP3/7 and TrCASP3/7 were incubated with Ac-DAVD-ρNA or Ac-DMPD-ρNA at 37°C for 30 min, and the proteolytic activity was determined. Data are expressed as the means ± SD of three replicates. **(C)** Structure analysis of the linker region from HsGSDME and TrGSDME with moue GSDMA3 (PDB:5b5r) as the template. Two regions that may form α-helix and loop are indicated. **(D)** HsGSDME wild type (WT) and mutants (Δ261-266 and Δ281-296) were treated with or without 1 U of HsCASP3/7 for 2 h, and the cleaved fragments were subjected to immunoblotting with anti-HsGSDME-CT antibody. **(E)** Schematics of the chimeric GSDME constructs. **(F-I)** TrGSDME (F), HsNT-TrCT (G), HsGSDME (H) and TrNT-HsCT (I) were incubated with 1 U of TrCASP3/7 or HsCASP3/7 for 2 h, and the cleavage was determined by immunoblotting with anti-TrGSDME or anti-HsGSDME-CT antibodies. For panels (A, D, and F-I): FL, full length; NT, N-terminal fragment; CT, C-terminal fragment.

Figure 4. The p10 subunit of CASP7 is essential for discrimination on GSDME. (A) Sequence alignment of HsCASP7 and TrCASP7 with HsCASP7 (PDB:1K86) as the template. α-helices and β-strands are indicated. The motifs involved in catalytic reaction (SHG and QACRG) and substrate binding (SWR and GSWF) are boxed in red. **(B)** Schematics of CASP7 chimeras. **(C)** The proteolytic activities of TrCASP7, HsCASP7 and their chimeras were determined by cleaving Ac-DAVD-ρNA and Ac-

DMPD-ρNA. Data are expressed as the means ± SD of three replicates. **(D-G)** TrGSDME (D), HsNT-TrCT (E), HsGSDME (F) or TrNT-HsCT (G) were incubated with TrCASP7, HsCASP7 and their chimeras for 2 h. The products were assessed by immunoblotting with anti-TrGSDME or anti-HsGSDME-CT antibodies. For panels (D-G): FL, full length; NT, N-terminal fragment; CT, C-terminal fragment.

Figure 5. Functional importance of the non-conserved residues in the p10 of HsCASP7 and TrCASP7. (A) Sequence alignment of the p10 region in HsCASP7 and TrCASP7. The arrows indicate non-conserved residues. **(B, C)** HsGSDME was treated with wild type (WT) or mutant HsCASP7 (B) or TrCASP7 (C) for 2 h. The cleavage was determined by immunoblotting with anti-HsGSDME-CT antibody. 205TME, HsCASP7 with TME insertion at position 205; 213ΔTME, TrCASP7 with TME deleted at position 213. **(D, E)** TrGSDME was incubated with wild type (WT) or mutant HsCASP7 (D) or TrCASP7 (E) for 2 h. The cleavage was determined by immunoblotting with anti-TrGSDME antibody. **(F)** HsGSDME was incubated with HsCASP7 or the S234N mutant (0.25-4U) for 2 h. HsGSDME cleavage was analyzed as above. **(G, H)** HsGSDME (G) and TrGSDME (H) were treated with wild type or mutant HsCASP7 for 2 h. The cleavage was determined as above. **(I, J)** TrGSDME (I) or HsGSDME (J) was co-expressed with wild type or mutant TrCASP7/HsCASP7 for 24 h. GSDME cleavage, CASP7 and β-actin were determined as above. **(K)** HsGSDME was co-expressed with HsCASP7 or HsCASP7-S234N for 48 h. Cleavage of GSDME was detected as above. For panels (B-K): FL, full length; NT, N-terminal fragment; CT, C-terminal fragment.

Figure 6. Conservation and functional importance of S/N234 in CASP3/7. (A) Weblogo analysis of the conservation of S/N234 in CASP3/7 in Mammalia, Aves, Reptilia, Amphibia and Osteichthyes. **(B)** Sequence alignment of HsCASP3/7. The S/N residues are indicated by red arrow. **(C)** HsGSDME was treated with HsCASP3 or HsCASP3-N208S for 2 h, and then subjected to immunoblotting with anti-HsGSDME-CT antibody. **(D)** HsGSDME was co-expressed in HEK293T cells with different doses of HsCASP3 or HsCASP3-N208S for 24 h. The cell lysates were immunoblotted to

detect HsGSDME, CASP3, and β-actin. **(E)** Sequence alignment of the S/N234 region in the CASP7 of primate (shaded cyan) and non-primate mammals. The S/N residues are indicated by red arrow. Asterisks indicate identical residues. **(F)** Alignment of human and mouse CASP7 sequences. The S/N234 residues are indicated by arrow. **(G)** HsGSDME was treated with different units of HsCASP7 or MmCASP7 for 2 h, and the cleavage was assessed by immunoblotting with anti-HsGSDME-CT antibody. **(H)** HsGSDME was incubated with different units of MmCASP7 or its mutant (N234S) for 2 h, and HsGSDME cleavage was analyzed as above. **(I)** MmCASP7 was treated with HsCASP7, MmCASP7 or MmCASP7-N234S for 2 h. The cleavage was determined by immunoblotting with anti-MmGSDME-NT antibody. For panels (C, D, and G-I), FL, full length; NT, N-terminal fragment; CT, C-terminal fragment.

Figure 1-figure supplement 1. Phylogenetic analysis of the TrGSDME used in this study. The phylogenetic tree was constructed using 15 fish GSDMEa (red) and 51 fish GSDMEb (blue) collected from NCBI databank. The TrGSDME used in this study is indicated by a red star.

Figure 1-figure supplement 2. Cleavage of TrGSDME mutants by HsCASP3/7. TrGSDME wild type (WT) and mutants (D255R and D258A) were treated with or without (-) HsCASP3/7 for 2 h, and the cleavage was determined by immunoblotting with anti-His antibody. FL, full length; CT, cleaved C-terminal region.

Figure 2-figure supplement 1. Ectopic expression of TrGSDME-FL and truncates. HEK293T cells were transfected with the backbone vector or the vector expressing mCherry-tagged TrGSDME full length (FL) or truncates (NT or CT) for 24 h. The cell lysate was then immunoblotted with antibody against mCherry or β-actin.

Figure 2-figure supplement 2. The cell death-inducing ability of TrGSDME-FL and truncates. HEK293T cells were transfected with the backbone vector or the vector expressing mCherry-tagged TrGSDME full length (FL) or truncate (NT or CT) for 24 h. The cells were then stained with Sytox Green and examined with a microscope. Scale bar, 30 μm.

Figure 2-figure supplement 3. Activation of TrGSDME-mediated pyroptosis by TrCASP3/7. (A) HEK293T cells were transfected with the backbone vector or the vector expressing the indicated protein for 24 h and then stained with Sytox Green. Scale bars, 30 μm. **(B, C)** HEK293T cells expressing wild type (WT) or mutant TrGSDME together with or without (control) TrCASP3 or TrCASP7 were subjected to Sytox Green staining (B) and TrGSDME cleavage analysis by immunoblot with antibodies against mCherry (upper), Myc (middle), and actin (lower) (C). Scale bar, 30 μm.

Figure 3-figure supplement 1. Cleavage of HsGSDME by caspases. Recombinant HsGSDME was incubated with or without (-) HsCASP1, 2, 3, 6, 7, 8, and 9 for 2 h, and the cleavage was determined by SDS-PAGE. M, molecular markers. FL, full length; NT, N-terminal fragment; CT, C-terminal fragment.

Figure 3-figure supplement 2. Proteolytic activity of TrCASP1. TrCASP1 was incubated with colorimetric Ac-YVAD-ρNA, Ac-DAVD-ρNA, and Ac-DMPD-ρNA for 1 h, and the cleavage was determined by measuring the release of ρNA. Values are the means of triplicate experiments and shown as means ± SD..

Figure 4-figure supplement 1. Preparation of recombinant proteins. (A) SDS-PAGE analysis of purified Hsp20-Trp10 and Trp20-Hsp10. **(B, C)** Purified TrCASP7 (B) and HsCASP7 (C) were subjected to SDS-PAGE (upper panel) and immunoblotting with anti-His tag antibody (lower panel). **(D)** HsCASP3 and its mutant (N208S) were analyzed by SDS-PAGE. **(E)** SDS-PAGE analysis of purified MmCASP7 and its mutant (N234S). In all panels, the p10 and p20 subunits are indicated.

Figure 5-figure supplement 1. Cleavage of poly (ADP-ribose) polymerase 1 (PARP1) and gelsolin by HsCASP7. HEK293T cells were transfected with C-terminal Flag-tagged PARP1 (left panel) or gelsolin (right panel) for 24 h. The cell lysates were incubated with or without (-) different units of HsCASP7 and HsCASP7-S234N for 2 h and then subjected to immunoblotting with anti-Flag antibody.

Figure 5-figure supplement 2. Structural analysis of HsCASP1/4/7. (A) The structures of HsCASP1 (PDB: 6kn0, gray), HsCASP4 (PDB: 6kmz, green), and HsCASP7 (PDB: 6kn0, purple) are superimposed. The βIII/βIII' sheets of HsCASP1/4 are indicated by arrows; the residues Q276, D278, and H283 of HsCASP7 are shown in cyan. **(B)** The sequence alignment of HsCASP1/4 βIII/βIII' sheet with the corresponding region of HsCASP7.

Figure 5-figure supplement 3. GSDME cleavage by CASP7 in cellular system. TrGSDME (A) or HsGSDME (B) was co-expressed with different doses of TrCASP7/HsCASP7 for 48 h in HEK293T cells. The expression/cleavage of

TrGSDME/HsGSDME and the expression of TrCASP7/HsCASP7 were determined by immunoblotting. β-actin was used as a loading control.

Figure 6-figure supplement 1. Conservation of S/N234 in mammalian CASP7. The four conserved amino acids are shown in LOGOs, with height representing the relative proportion of the corresponding amino acid at that position. The S/N234 is presented as the fourth LOGO and indicated with a red star.

Figure 6-figure supplement 2. The cleavage of MmGSDME by MmCASP3. (A) SDS-PAGE analysis of purified MmCASP3. **(B)** MmGSDME was treated with 1U of MmCASP3 for 2 h and then subjected to SDS-PAGE.

Legends for Figure 1-video 1:

Figure 1-video 1 (separate file). TrGSDME-NT induces pyroptosis of HEK293T cells. HEK293T cells were transfected with the vector expressing mCherry-tagged TrGSDME-NT, and time-lapse images of the cells were recorded with a confocal microscope.

Tables

Table 1. The CASP3 sequences used for WebLogo analysis in this study.

Class	Species	Accession Number
Mammalia	*Homo sapiens*	P42574
	Mus musculus	P70677
	Sus scrofa	Q95ND5
	Canis lupus familiaris	Q8MKI5
	Saimiri boliviensis	NP_001266895.1
	Equus caballus	NP_001157433.1
	Mesocricetus auratus	Q60431
	Pan troglodytes	XP_009446811.1
	Ovis aries	XP_014960045.1
	Capra hircus	NP_001273018.1
	Pan paniscus	XP_003823509.1
	Ailuropoda melanoleuca	XP_002914062.1
	Oryctolagus cuniculus	Q8MJC3
	Loxodonta africana	XP_023410784.1
	Bos taurus	Q08DY9
	Macaca fascicularis	Q2PFV2
	Delphinapterus leucas	XP_022426661.1
	Aotus nancymaae	XP_012327995.1
	Vulpes vulpes	XP_025874057.1

	Heterocephalus glaber	EHB15384.1
	Bos mutus grunniens	XP_010834058.1
	Balaenoptera acutorostrata	XP_007177921.2
	Odobenus rosmarus divergens	XP_012422221.1
	Tursiops truncatus	XP_033704658.1
	Saimiri boliviensis	AAV74267.1
	Theropithecus gelada	XP_025242051.1
	Rhinopithecus roxellana	XP_010376231.2
	Chlorocebus sabaeus	XP_007998582.1
	Arvicanthis niloticus	XP_034376775.1
	Castor canadensis	JAV41953.1
	Urocitellus parryii	XP_026256383.1
	Neogale vison	XP_044081570.1
	Lynx rufus	XP_046947013.1
	Canis lupus dingo	XP_025327613.1
	Balaenoptera acutorostrata scammoni	XP_007177921.1
	Balaenoptera musculus	XP_036694636.1
	Vicugna pacos	XP_006198038.1
	Camelus bactrianus	XP_010951604.1
	Eptesicus fuscus	XP_008150114.1
	Pteropus alecto	XP_006916432.1
	Ochotona princeps	XP_004579072.1
	Equus quagga	XP_046504640.1
	Talpa occidentalis	XP_037382298.1
	Manis pentadactyla	XP_036750218.1
	Gracilinanus agilis	XP_044536929.1
Aves	*Corvus hawaiiensis*	XP_048160132.1
	Taeniopygia guttata	XP_030127125.3

Pyrgilauda ruficollis	XP_041335801.1
Hirundo rustica	XP_039921773.1
Onychostruthus taczanowskii	XP_041283907.1
Passer montanus	XP_039555833.1
Molothrus ater	XP_036238378.1
Oxyura jamaicensis	XP_035179722.1
Melopsittacus undulatus	XP_030904860.1
Strigops habroptila	XP_030349011.1
Aythya fuligula	XP_032043173.1
Lonchura striata domestica	OWK64686.1
Geospiza fortis	XP_005415590.1
Camarhynchus parvulus	XP_030803986.1
Serinus canaria	XP_030094646.1
Manacus vitellinus	XP_008923018.1
Zonotrichia albicollis	XP_005483896.1
Apteryx rowi	XP_025939844.1
Numida meleagris	XP_021249041.1
Gallus gallus	NP_990056.1
Tyto alba	XP_042663613.1
Lagopus leucura	XP_042726563.1
Pygoscelis adeliae	XP_009328950.1
Calypte anna	XP_030305365.1
Aquila chrysaetos chrysaetos	XP_029861401.1
Haliaeetus leucocephalus	XP_010568301.1
Tyto alba	XP_032854868.1
Hirundo rustica	XP_039921766.1
Cygnus atratus	XP_035413755.1
Lepidothrix coronata	XP_017664322.1

	Amazona aestiva	KQK77628.1
	Chaetura pelagica	XP_010000752.1
	Antrostomus carolinensis	XP_010171751.1
	Nipponia nippon	XP_009473093.1
	Pelecanus crispus	XP_009479867.1
	Leptosomus discolor	XP_009958677.1
	Dryobates pubescens	XP_009909179.1
	Manacus vitellinus	XP_008923018.1
	Parus major	XP_015479949.1
	Falco rusticolus	XP_037254769.1
	Numida meleagris	XP_021249038.1
Reptilia	*Pelodiscus sinensis*	XP_006128559.1
	Gopherus evgoodei	XP_030419000.1
	Chelonia mydas	XP_043402007.1
	Dermochelys coriacea	XP_043369528.1
	Mauremys reevesii	XP_039396469.1
	Terrapene carolina triunguis	XP_029766549.1
	Trachemys scripta elegans	XP_034627282.1
	Python bivittatus	XP_025018785.1
	Pogona vitticeps	XP_020658385.1
	Zootoca vivipara	XP_034967628.1
	Podarcis muralis	XP_028600040.1
	Sceloporus undulatus	XP_042323800.1
	Lacerta agilis	XP_033017209.1
	Varanus komodoensis	XP_044305785.1
	Notechis scutatus	XP_026522951.1
	Pantherophis guttatus	XP_034257179.1
	Protobothrops mucrosquamatus	XP_015687286.1

	Eremias argus	QCQ80689.1
	Sceloporus undulatus	XP_042323800.1
	Gekko japonicus	XP_015272894.1
	Lacerta agilis	XP_033017209.1
	Notechis scutatus	XP_026522951.1
	Pseudonaja textilis	XP_026553662.1
	Sphaerodactylus townsendi	XP_048364960.1
	Thamnophis sirtalis	XP_013910221.1
	Crotalus tigris	XP_039186723.1
	Thamnophis elegans	XP_032080611.1
	Crocodylus porosus	XP_019390228.1
	Chelonoidis abingdonii	XP_032656285.1
	Chrysemys picta bellii	XP_005282030.1
	Mauremys mutica	XP_044873973.1
Amphibia	*Xenopus laevis*	NP_001081225.1
	Bufo gargarizans	XP_044145804.1
	Rana temporaria	XP_040189928.1
	Bufo bufo	XP_040274658.1
	Geotrypetes seraphini	XP_033799250.1
	Microcaecilia unicolor	XP_030047368.1
	Nanorana parkeri	XP_018421176.1
	Cynops orientalis	AFN55260.1
	Xenopus tropicalis	NP_001120900.1
	Rhinatrema bivittatum	XP_029441076.1
	Geotrypetes seraphini	XP_033799250.1
Osteichthyes	*Paralichthys olivaceus*	XP_019958716.1
	Danio rerio	AWP39888.1
	Dicentrarchus labrax	ABC70997.1

Larimichthys crocea	NP_001290322.1
Scophthalmus maximus	AVW89178.1
Cynoglossus semilaevis	XP_016894801.1
Cyprinus carpio	XP_018965718.1
Cyprinodon variegatus	XP_015245088.1
Cyprinodon tularosa	XP_038127805.1
Takifugu rubripes	NP_001027871.1
Salmo salar	NP_001133393.1
Oncorhynchus mykiss	BAU69680.1
Monopterus albus	XP_020451082.1
Nothobranchius furzeri	KAF7225424.1
Miichthys miiuy	AHG06618.1
Anguilla japonica	AYC61977.1
Scleropages Formosus	XP_018591577.1
Poecilia reticulata	XP_008417983.1
Poecilia formosa	XP_007549682.1
Oplegnathus fasciatus	AFM09714.1
Collichthys lucidus	TKS72762.1
Notothenia coriiceps	XP_010794822.1
Poeciliopsis prolifica	JAO80483.1
Haplochromis burtoni	XP_005944370.2
Cyprinus carpio	AGU12796.1
Cyprinus carpio	AGU12795.1
Electrophorus electricus	XP_026884624.2
Amphiprion melanopus	AEA08874.1
Archocentrus centrarchus	XP_030591190.1
Bagarius yarrelli	TSN95700.1
Oryzias melastigma	XP_024138660.1

	Oryzias latipes	NP_001098140.1
	Siniperca chuatsi	ADK47519.1
	Kryptolebias marmoratus	XP_017278585.1
	Astyanax mexicanus	XP_022539261.1
	Miichthys miiuy	AHG06618.1
	Xiphophorus couchianus	XP_027872889.1
	Oreochromis niloticus	ADJ57601.1
	Lutjanus peru	QBY35776.1
	Mugil incilis	QDK54780.1

837
838

839 **Table 2. The CASP7 sequences used for the WebLogo analysis in this study.**

Class	Species	Accession Number
Mammalia	*Homo sapiens*	P55210
	Mus musculus	P97864
	Mesocricetus auratus	P55214
	Bos taurus	XP_002698555.1
	Pan troglodytes	XP_003825650.1
	Macaca fascicularis	XP_011822901.1
	Oryctolagus cuniculus	XP_002718761.1
	Ovis aries	XP_042094975.1
	Capra hircus	XP_005698554.1
	Ailuropoda melanoleuca	XP_034519188.1
	Saimiri boliviensis boliviensis	XP_034519188.1
	Equus caballus	XP_014588811.1
	Delphinapterus leucas	XP_022424428.1
	Sus scrofa	XP_020928977.1
	Pan paniscus	XP_003825650.1
	Loxodonta africana	XP_010587277.1
	Canis lupus familiaris	XP_005637795.1
	Oryctolagus cuniculus	XP_002718761.1
	Vulpes vulpes	XP_025849552.1
	Heterocephalus glaber	XP_004838949.1
	Urocitellus parryii	XP_026244955.1
	Equus asinus	XP_014723324.1
	Tachyglossus aculeatus	XP_038614071.1
	Camelus bactrianus	XP_010968130.1
	Balaenoptera acutorostrata scammoni	XP_007173176.1
	Myodes glareolus	XP_048279394.1
	Dipodomys spectabilis	XP_042545561.1

	Delphinapterus leucas	XP_022424428.1
	Eptesicus fuscus	XP_028005288.1
	Bison bison bison	XP_010857610.1
	Pteropus alecto	XP_006920912.1
	Rhinopithecus bieti	XP_017747992.1
	Balaenoptera musculus	XP_036685506.1
	Saimiri boliviensis boliviensis	XP_010331177.1
	Myotis brandtii	XP_005874576.1
	Ursus americanus	XP_045659135.1
	Neogale vison	XP_044096500.1
	Vulpes lagopus	XP_041601933.1
	Equus quagga	XP_046510739.1
	Oryctolagus cuniculus	XP_002718761.1
	Galemys pyrenaicus	KAG8517409.1
	Manis pentadactyla	XP_036754817.1
	Gracilinanus agilis	XP_044521530.1
Aves	*Corvus hawaiiensis*	XP_048166914.1
	Taeniopygia guttata	XP_030132303.3
	Pyrgilauda ruficollis	XP_041317496.1
	Hirundo rustica	XP_039927077.1
	Onychostruthus taczanowskii	XP_041271849.1
	Passer montanus	XP_039565350.1
	Molothrus ater	XP_036241577.1
	Oxyura jamaicensis	XP_035186324.1
	Turdus rufiventris	KAF4791228.1
	Melopsittacus undulatus	XP_005154576.1
	Strigops habroptila	XP_030344254.1
	Aythya fuligula	XP_032047208.1

Lonchura striata domestica	XP_021381698.1
Geospiza fortis	XP_005416425.1
Camarhynchus parvulus	XP_030807062.1
Serinus canaria	XP_009085424.1
Manacus vitellinus	XP_029814357.1
Zonotrichia albicollis	XP_005481147.1
Apteryx rowi	XP_025925619.1
Numida meleagris	XP_021255526.1
Gallus gallus	XP_040530979.1
Tyto alba	XP_032844696.2
Lagopus leucura	XP_042719653.1
Pygoscelis adeliae	XP_009324216.1
Corvus brachyrhynchos	XP_008632648.1
Calypte anna	XP_030309482.1
Apteryx mantelli mantelli	XP_013797196.1
Apaloderma vittatum	XP_009876249.1
Haliaeetus leucocephalus	XP_010563034.1
Tyto alba	XP_032844693.2
Lonchura striata domestica	OWK56987.1
Cygnus atratus	XP_035403725.1
Cyanistes caeruleus	XP_023785639.1
Amazona aestiva	KQK80332.1
Mesitornis unicolor	XP_010180183.1
Melopsittacus undulatus	XP_005154576.1
Athene cunicularia	XP_026707509.1
Camarhynchus parvulus	XP_030807062.1
Gallus gallus	XP_421764.3
Chaetura pelagica	XP_010006222.1

	Ficedula albicollis	XP_005048826.1
	Serinus canaria	XP_009085424.1
	Cuculus canorus	XP_009568871.1
	Corvus cornix cornix	XP_039410202.1
	Nipponia nippon	XP_009474328.1
	Pelecanus crispus	XP_009483464.1
	Balearica regulorum gibbericeps	XP_010295946.1
	Manacus vitellinus	XP_017924402.1
	Phalacrocorax carbo	XP_009508983.1
	Parus major	XP_015489222.1
	Falco rusticolus	XP_037256573.1
	Corvus hawaiiensis	XP_048166914.1
Reptilia	*Pelodiscus sinensis*	XP_006135034.1
	Gopherus evgoodei	XP_030424754.1
	Chelonia mydas	XP_037760318.1
	Dermochelys coriacea	XP_038265833.1
	Mauremys reevesii	XP_039402417.1
	Terrapene carolina triunguis	XP_026506928.1
	Trachemys scripta elegans	XP_034632909.1
	Python bivittatus	XP_007441954.1
	Pogona vitticeps	XP_020635566.1
	Zootoca vivipara	XP_034988803.1
	Podarcis muralis	XP_028586060.1
	Sceloporus undulatus	XP_042313006.1
	Anolis carolinensis	XP_008112942.1
	Varanus komodoensis	KAF7253514.1
	Lacerta agilis	XP_033005524.1
	Notechis scutatus	XP_026526250.1

	Notechis scutatus	XP_026526259.1
	Pantherophis guttatus	XP_034296056.1
	Python bivittatus	XP_007441954.1
	Protobothrops mucrosquamatus	XP_015676047.1
	Zootoca vivipara	XP_034988803.1
	Podarcis muralis	XP_028586060.1
	Sceloporus undulatus	XP_042313006.1
	Anolis carolinensis	XP_003223489.1
	Varanus komodoensis	KAF7253514.1
	Varanus komodoensis	XP_044295172.1
	Lacerta agilis	XP_033005524.1
	Notechis scutatus	XP_026526250.1
	Pantherophis guttatus	XP_034296056.1
	Protobothrops mucrosquamatus	XP_015676047.1
	Pseudonaja textilis	XP_026560589.1
	Sphaerodactylus townsendi	XP_048360798.1
	Crotalus tigris	XP_039208641.1
	Thamnophis elegans	XP_032081709.1
	Chelonoidis abingdonii	XP_032631043.1
	Mauremys mutica	XP_044881213.1
	Chrysemys picta bellii	XP_042711209.1
	Trachemys scripta elegans	XP_034632910.1
	Crocodylus porosus	XP_019411759.1
Amphibia	*Xenopus laevis*	BAA94748.1
	Lithobates catesbeianus	ACO51875.1
	Bufo gargarizans	XP_044152860.1
	Rana temporaria	XP_040217514.1
	Bufo bufo	XP_040291577.1

	Geotrypetes seraphini	XP_033799427.1
	Microcaecilia unicolor	XP_030058570.1
	Nanorana parkeri	XP_018419981.1
	Cynops orientalis	AFN55259.1
	Xenopus tropicalis	NP_001016299.1
	Xenopus tropicalis	CAJ82745.1
	Rhinatrema bivittatum	XP_029466303.1
Osteichthyes	*Paralichthys olivaceus*	XP_019965790.1
	Danio rerio	AWP39893.1
	Dicentrarchus labrax	CBN81450.1
	Larimichthys crocea	XP_010740374.1
	Scophthalmus maximus	XP_047183439.1
	Cynoglossus semilaevis	XP_024912944.1
	Oncorhynchus kisutch	XP_020329675.1
	Cyprinus carpio	XP_042591656.1
	Cyprinodon variegatus	XP_015245976.1
	Fundulus heteroclitus	XP_012710613.2
	Cyprinodon tularosa	XP_029690759.1
	Takifugu rubripes	XP_029690759.1
	Salmo salar	XP_014012537.2
	Oncorhynchus mykiss	QWC93456.1
	Ictalurus punctatus	XP_017338665.1
	Monopterus albus	XP_020460887.1
	Nothobranchius furzeri	KAF7204369.1
	Alosa alosa	XP_048088911.1
	Alosa sapidissima	XP_041939757.1
	Anabarilius grahami	ROI81868.1
	Salvelinus alpinus	XP_023842909.1

Salvelinus alpinus	XP_023861943.1
Gadus morhua	XP_030195895.1
Labrus bergylta	XP_020506858.1
Toxotes jaculatrix	XP_040923277.1
Collichthys lucidus	TKS89629.1
Notothenia coriiceps	XP_010765636.1
Melanotaenia boesemani	XP_041830322.1
Clarias magur	KAF5896512.1
Anabas testudineus	XP_026207209.1
Chelmon rostratus	XP_041817955.1
Anguilla anguilla	XP_035260198.1
Trematomus bernacchii	XP_033975792.1
Pimephales promelas	KAG1954935.1
Bagarius yarrelli	TSK14754.1
Seriola dumerili	XP_022598445.1
Xiphophorus hellerii	XP_032429481.1
Sebastes umbrosus	XP_037611938.1
Parambassis ranga	XP_028285718.1
Oryzias melastigma	KAF6724972.1
Megalops cyprinoides	XP_036387401.1
Salarias fasciatus	XP_029954337.1
Salvelinus namaycush	XP_038866282.1

840
841

842 **Table 3. The credits for the pictures used in this study.**

Icon	Figure Origin
Monotremata	Becky-Barnes
Didelphimorphia	Daniel-Stadtmauer
Diprotodontia	Gavin-Prideaux
Afrosoricida	Mo-Hassan
Macroscelidea	uncredited
Pilosa	Xavier-A-Jenkins
Primates	T-Michael-Keesey
Rodentia	Jiro-Wada
Lagomorpha	Margot-Michaud
Eulipotyphla	Becky-Barnes
Perissodactyla	Mercedes-Yrayzoz-vectorized-by-T-Michael-Keesey
Artiodactyla	DFoidl-modified-by-T-Michael-Keesey
Carnivora	Chlo-Schmidt
Pholidota	Steven-Traver
Chiroptera	Margot-Michaud
Homo sapiens	NASA
Avian	Ferran Sayol
Reptilia	Gabriela Palomo-Munoz
Amphibia	Yusan Yang
Actinopterygii	Milton Tan

843

844 **Table 4. The constructs of the truncate and chimeric proteins.**

Truncate/chimeric protein	Amino acid sequence
TrGSDME-NT	1-258 aa of TrGSDME
TrGSDME-CT	259-474 aa of TrGSDME
HsNT-TrCT	1-270 aa of HsGSDME + 259-274 aa of TrGSMDE
TrNT-HsCT	1-258 aa of TrGSDME + 271-496 aa of HsGSDME
Hsp20-Trp10	1-198 aa of HsCASP7 + 207-313 aa of TrCASP7
Trp20-Hsp10	1-206 aa of TrCASP7 + 199-303 aa of HsCASP7

845
846
847

848 **Table 5. Primers used in this study.**

Primer	Sequence (5'-3')
Clone primers	
TrCASP3 forward	ATGTCGGCCAACGGACC
TrCASP3 reverse	GGAAAAATACATCTCTTTGGTCAGC
TrCASP7 forward	ATGCAGATGGCTGGAGAACC
TrCASP7 reverse	GTTAAAGTACAGTTCTTTTGTCAGCATCG
TrGSDME forward	ATGTTTTCCAAGGCCACGG
TrGSDME reverse	ATCGATAAAATCCGTTTCAGACTTTG
Recombiantion primers	
TrCASP3 forward	TAAGAAGGAGATATACATATGATGT
	CGGCCAACGGACC
TrCASP3 reverse	GTGGTGGTGGTGGTGCTCGAGGGA
	AAAATACATCTCTTTGGTCAGC
TrCASP7 forward	TAAGAAGGAGATATACATATGATGCA
	GATGGCTGGAGAACC
TrCASP7 reverse	GTGGTGGTGGTGGTGCTCGAGGTTAA
	AGTACAGTTCTTTTGTCAGCATCG

TrGSDME forward	TAAGAAGGAGATATACATATGATGTTT TCCAAGGCCACGG
TrGSDME reverse	GTGGTGGTGGTGGTGCTCGAGATCGA TAAAATCCGTTTCAGACTTTG
TrGSDME-D255R forward	TGGGAATCCCCGAGAGCGGTGGATGG TCGTTGTCT
TrGSDME-D255R reverse	AGACAACGACCATCCACCGCTCTCGG GGATTCCCA
TrGSDME-D258A forward	AGACAACGACCATCCACCGCTCTCGG GGATTCCCA
TrGSDME-D258A reverse	AACGACCATCCACCGCTCTCGGGGATT CCCA
HsNT-TrCT forward	TAAGAAGGAGATATACATATGATGTT TGCCAAAGCAACCAGG
HsNT-TrCT reverse	GTGGTGGTGGTGGTGCTCGAGATCG ATAAAATCCGTTTCAGACTTTG
TrNT-HsCT forward	TAAGAAGGAGATATACATATGATGTT TTCCAAGGCCACGG
TrNT-HsCT reverse	GTGGTGGTGGTGGTGCTCGAGTGAA TGTTCTCTGCCTAAAGC
Hsp20-Trp10 forward	TAAGAAGGAGATATACATATGATGG CAGATGATCAGGGCTG
Hsp20-Trp10 reverse	GTGGTGGTGGTGGTGCTCGAGGTTA AAGTACAGTTCTTTTGTCAGCATC
Trp20-Hsp10 forward	TAAGAAGGAGATATACATATGATGG CTGGAGAACCCACTGAG
Trp20-Hsp10 reverse	GTGGTGGTGGTGGTGCTCGAGTTGA CTGAAGTAGAGTTCCTTGGTGA

MmGSDME-N234S forward	GTTATTACTCATGGAGGAGCCCAGG GAAAG
MmGSDME-N234S reverse	CTTTCCCTGGGCTCCTCCATGAGTA ATAAC
HsGSDME-Δ261-266 forward	CCAGGATGGACATCCATTTGCGGAG CTGC
HsGSDME-Δ261-266 reverse	CAAATGGATGTCCATCCTGGGAAGAT ATCCCAT
HsGSDME-Δ281-296 forward	CCTGGTCTTT GACATGCCAGATGCTG CGCA
HsGSDME-Δ281-296 reverse	CTGGCATGTCAAAGACCAGGGGGTCC AGGTAGA
Overexpression preimers	
TrGSDME-FL forward	TCAGATCTCGAGCTCAAGCTTATGTTT TCCAAGGCCACGG
TrGSDME-FL reverse	CATGGTGGCGACCGGTGGATCATCGA TAAAATCCGTTTCAGACTTTG
TrGSDME-NT forward	TCAGATCTCGAGCTCAAGCTTATGTTT TCCAAGGCCACGG
TrGSDME-NT reverse	CATGGTGGCGACCGGTGGATCGTCTAC AGCATCAGGAGACTCC
TrGSDME-CT forward	TCAGATCTCGAGCTCAAGCTTATGGGCC GGTGCCTGGA
TrGSDME-CT reverse	CATGGTGGCGACCGGTGGATCATCGA TAAAATCCGTTTCAGACTTTG
TrCASP7 forward	TTCTGAAGAGGACTTGAATTCAATGG CTGGAGAACCCACTGAG
TrCASP7 reverse	ACGACTCACTATAGTTCTAGATCAGT

	TAAAGTACAGTTCTTTTGTCAGC
TrCASP3 forward	TTCTGAAGAGGACTTGAATTCAAATG
	TCGGCCAACGGACC
TrCASP3 reverse	ACGACTCACTATAGTTCTAGAGGAA
	AAATACATCTCTTTGGTCAGC
HsGSDME forward	CAAGCTTGCGGCCGCGAATTCAATGT
	TTGCCAAAGCAACCAGG
HsGSDME reverse	ACGACTCACTATAGTTCTAGATCATG
	AATGTTCTCTGCCTAAAGC
HsCASP7 forward	TTCTGAAGAGGACTTGAATTCAATGG
	CAGATGATCAGGGCTG
HsCASP7 reverse	ACGACTCACTATAGTTCTAGACTATTG
	ACTGAAGTAGAGTTCCTTGGTG
HsCASP3 forward	TTCTGAAGAGGACTTGAATTCAATGG
	AGAACACTGAAAACTCAGTGG
HsCASP3 reverse	ACGACTCACTATAGTTCTAGATTAGTG
	ATAAAAATAGAGTTCTTTTGTGAGC
MmCASP7 forward	TTCTGAAGAGGACTTGAATTCAATGA
	CCGATGATCAGGACTGTGC
MmCASP7 reverse	ACGACTCACTATAGTTCTAGATCAAC
	GGCTGAAGTACAGCTCTTTGG

849

Figure 1

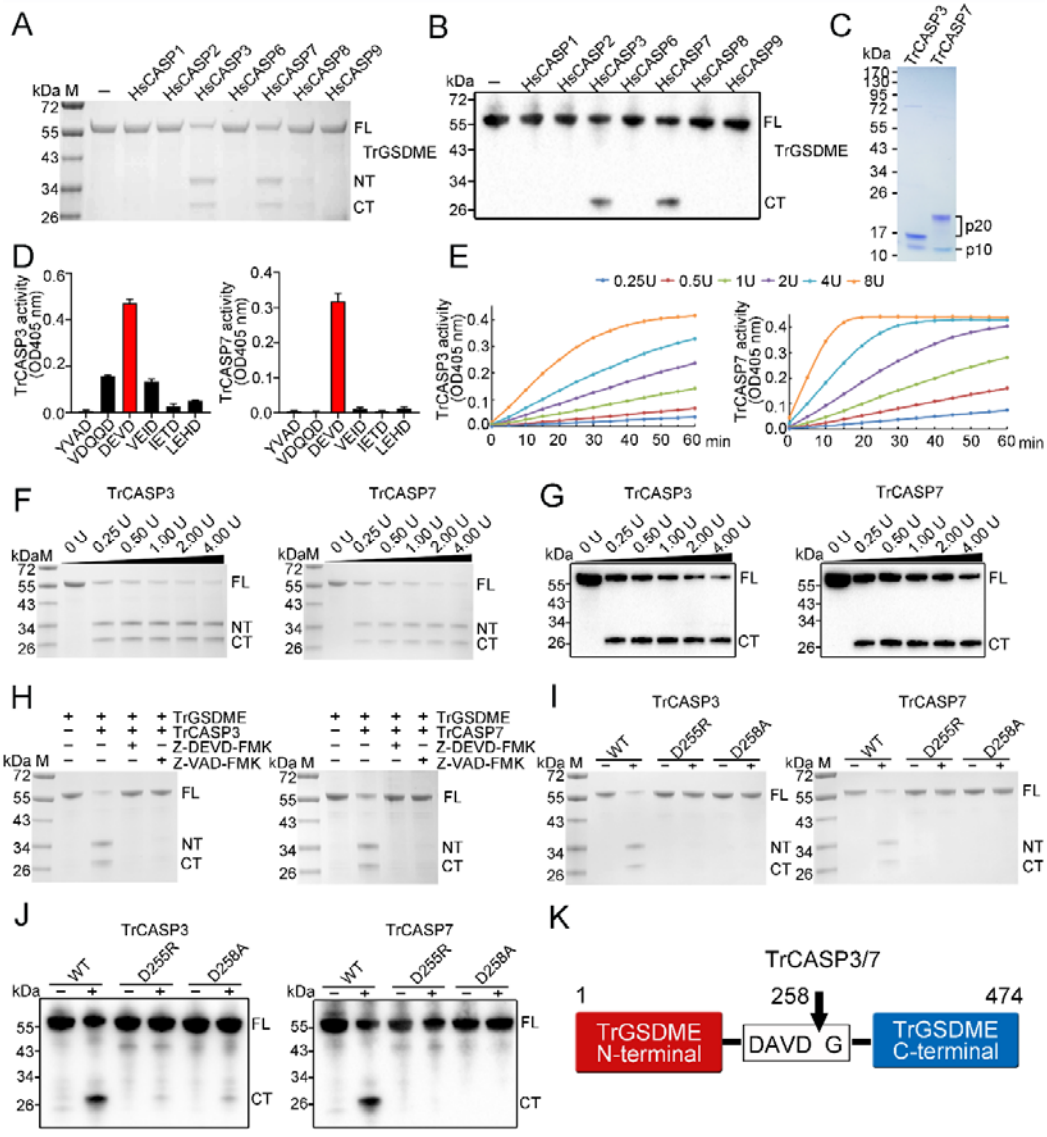
A
kDa M – HsCASP1 HsCASP2 HsCASP3 HsCASP6 HsCASP7 HsCASP8 HsCASP9
72
55
43
34
26
FL
TrGSDME
NT
CT
B
kDa – HsCASP1 HsCASP2 HsCASP3 HsCASP6 HsCASP7 HsCASP8 HsCASP9
72
55
43
34
26
FL
TrGSDME
CT
C
kDa TrCASP3 TrCASP7
170
130
95
72
55
43
34
26
17
10
p20
p10
D
TrCASP3 activity (OD405 nm)
0.6
0.4
0.2
0.0
TrCASP7 activity (OD405 nm)
0.4
0.3
0.2
0.1
0.0
YVAD VDQQD DEVD VEID IETD LEHD
E
0.25U 0.5U 1U 2U 4U 8U
TrCASP3 activity (OD405 nm)
TrCASP7 activity (OD405 nm)
0 10 20 30 40 50 60 min
F
TrCASP3
TrCASP7
kDaM 0 U 0.25 U 0.50 U 1.00 U 2.00 U 4.00 U
72
55
43
34
26
FL
NT
CT
G
TrCASP3
TrCASP7
kDa 0 U 0.25 U 0.50 U 1.00 U 2.00 U 4.00 U
55
43
34
26
FL
CT
H
TrGSDME
TrCASP3
Z-DEVD-FMK
Z-VAD-FMK
TrGSDME
TrCASP7
Z-DEVD-FMK
Z-VAD-FMK
kDa M
72
55
43
34
26
FL
NT
CT
I
TrCASP3
TrCASP7
kDa M WT D255R D258A
72
55
43
34
26
FL
NT
CT
J
TrCASP3
TrCASP7
kDa WT D255R D258A
55
43
34
26
FL
CT
K
TrCASP3/7
1
258
474
TrGSDME N-terminal
DAVD G
TrGSDME C-terminal

Figure 2

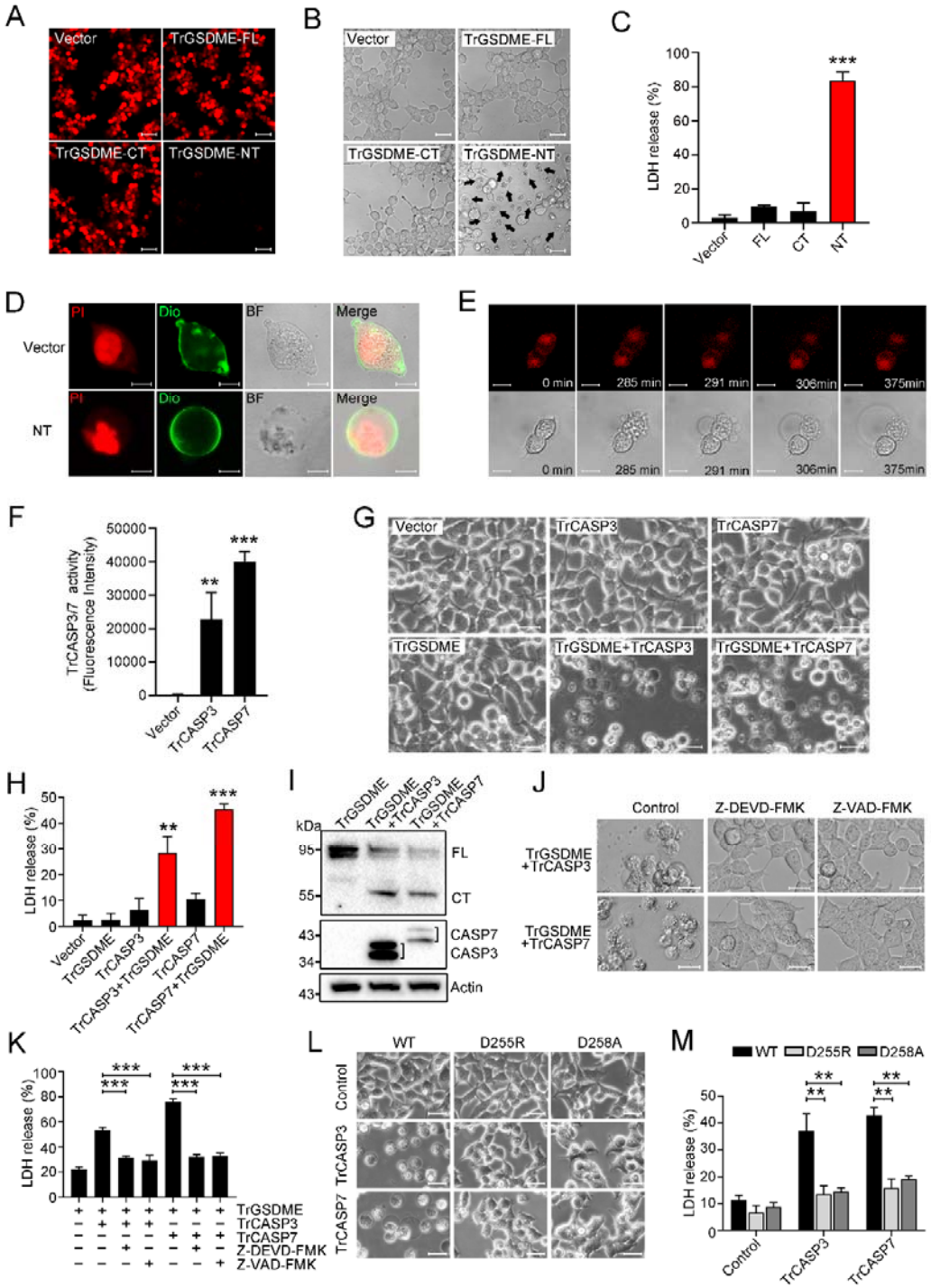
A
Vector
TrGSDME-FL
TrGSDME-CT
TrGSDME-NT
B
Vector
TrGSDME-FL
TrGSDME-CT
TrGSDME-NT
C
LDH release (%)
Vector
FL
CT
NT
***
D
PI
Dio
BF
Merge
Vector
NT
E
0 min
285 min
291 min
306min
375min
F
TrCASP3/7 activity (Fluorescence Intensity)
Vector
TrCASP3
TrCASP7
**
***
G
Vector
TrCASP3
TrCASP7
TrGSDME
TrGSDME+TrCASP3
TrGSDME+TrCASP7
H
LDH release (%)
Vector
TrGSDME
TrCASP3
TrCASP3+TrGSDME
TrCASP7
TrCASP7+TrGSDME
I
kDa
TrGSDME
TrGSDME +TrCASP3
TrGSDME +TrCASP7
95
55
43
34
FL
CT
CASP7
CASP3
Actin
J
Control
Z-DEVD-FMK
Z-VAD-FMK
TrGSDME +TrCASP3
TrGSDME +TrCASP7
K
LDH release (%)
TrGSDME
TrCASP3
TrCASP7
Z-DEVD-FMK
Z-VAD-FMK
L
WT
D255R
D258A
Control
TrCASP3
TrCASP7
M
WT
D255R
D258A
LDH release (%)
Control
TrCASP3
TrCASP7

Figure 3

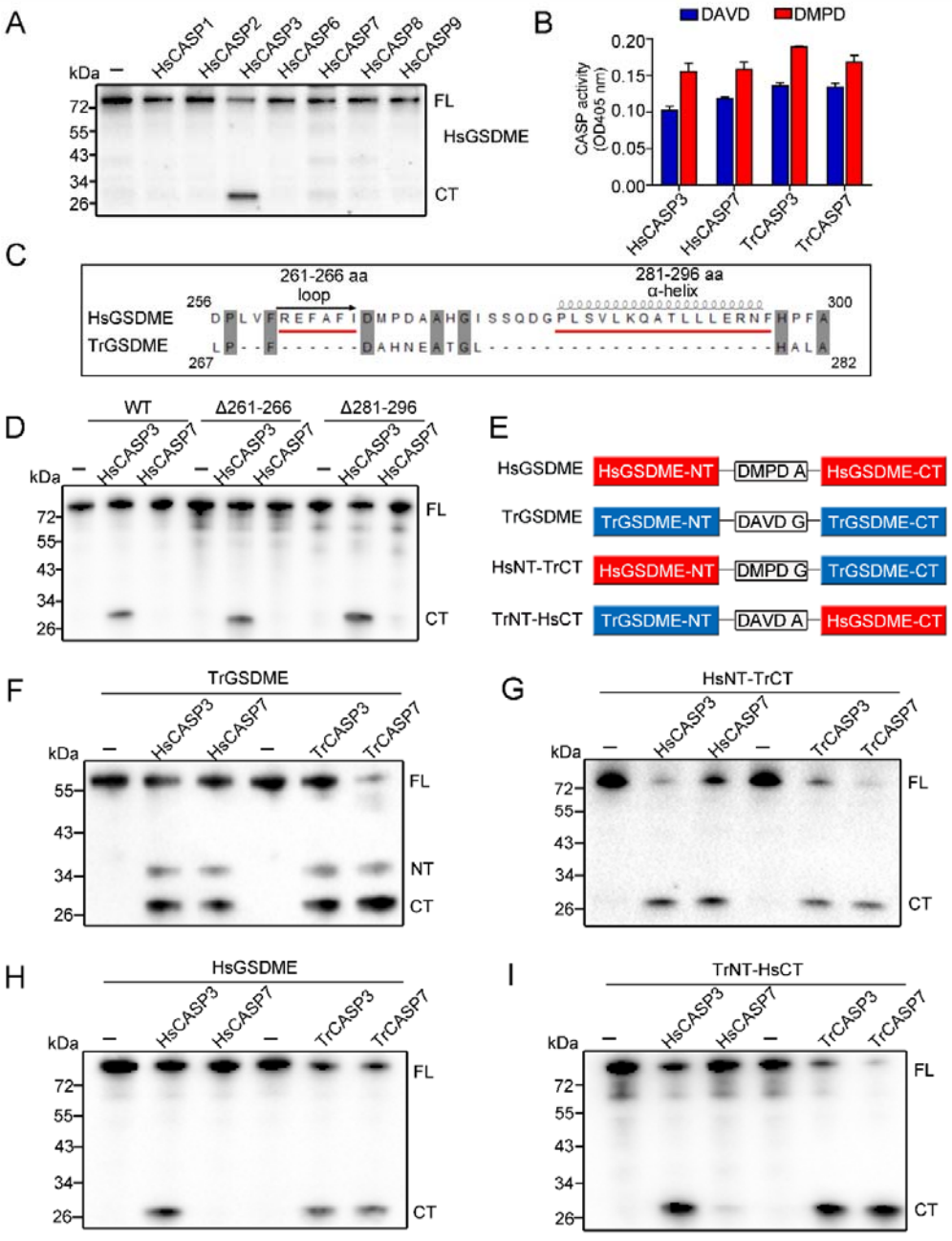
A
kDa
–
HsCASP1
HsCASP2
HsCASP3
HsCASP6
HsCASP7
HsCASP8
HsCASP9
72
55
43
34
26
FL
HsGSDME
CT
B
DAVD
DMPD
CASP activity (OD405 nm)
0.20
0.15
0.10
0.05
0.00
HsCASP3
HsCASP7
TrCASP3
TrCASP7
C
261-266 aa
loop
281-296 aa
α-helix
256
300
HsGSDME
TrGSDME
267
282
D
WT
Δ261-266
Δ281-296
HsCASP3
HsCASP7
FL
CT
E
HsGSDME
HsGSDME-NT
DMPD A
HsGSDME-CT
TrGSDME
TrGSDME-NT
DAVD G
TrGSDME-CT
HsNT-TrCT
DMPD G
TrNT-HsCT
DAVD A
F
TrGSDME
TrCASP3
TrCASP7
NT
G
HsNT-TrCT
H
HsGSDME
I
TrNT-HsCT

Figure 4

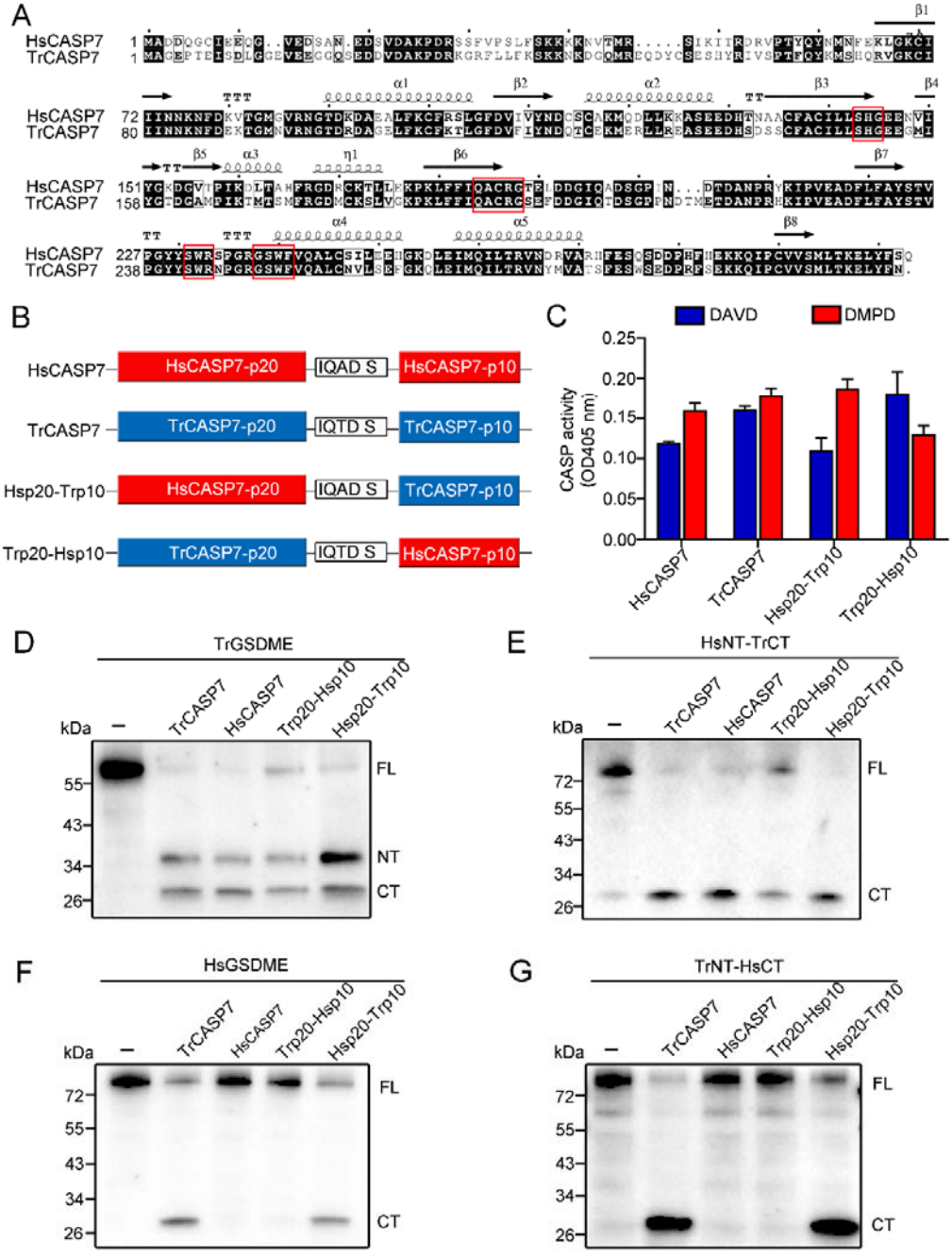
A
HsCASP7
TrCASP7
B
HsCASP7
HsCASP7-p20
IQAD S
HsCASP7-p10
TrCASP7
TrCASP7-p20
IQTD S
TrCASP7-p10
Hsp20-Trp10
Trp20-Hsp10
C
DAVD
DMPD
CASP activity (OD405 nm)
0.25
0.20
0.15
0.10
0.05
0.00
HsCASP7
TrCASP7
Hsp20-Trp10
Trp20-Hsp10
D
TrGSDME
kDa
–
TrCASP7
HsCASP7
Trp20-Hsp10
Hsp20-Trp10
55
43
34
26
FL
NT
CT
E
HsNT-TrCT
72
55
43
34
26
FL
CT
F
HsGSDME
72
55
43
34
26
FL
CT
G
TrNT-HsCT
72
55
43
34
26
FL
CT

Figure 5

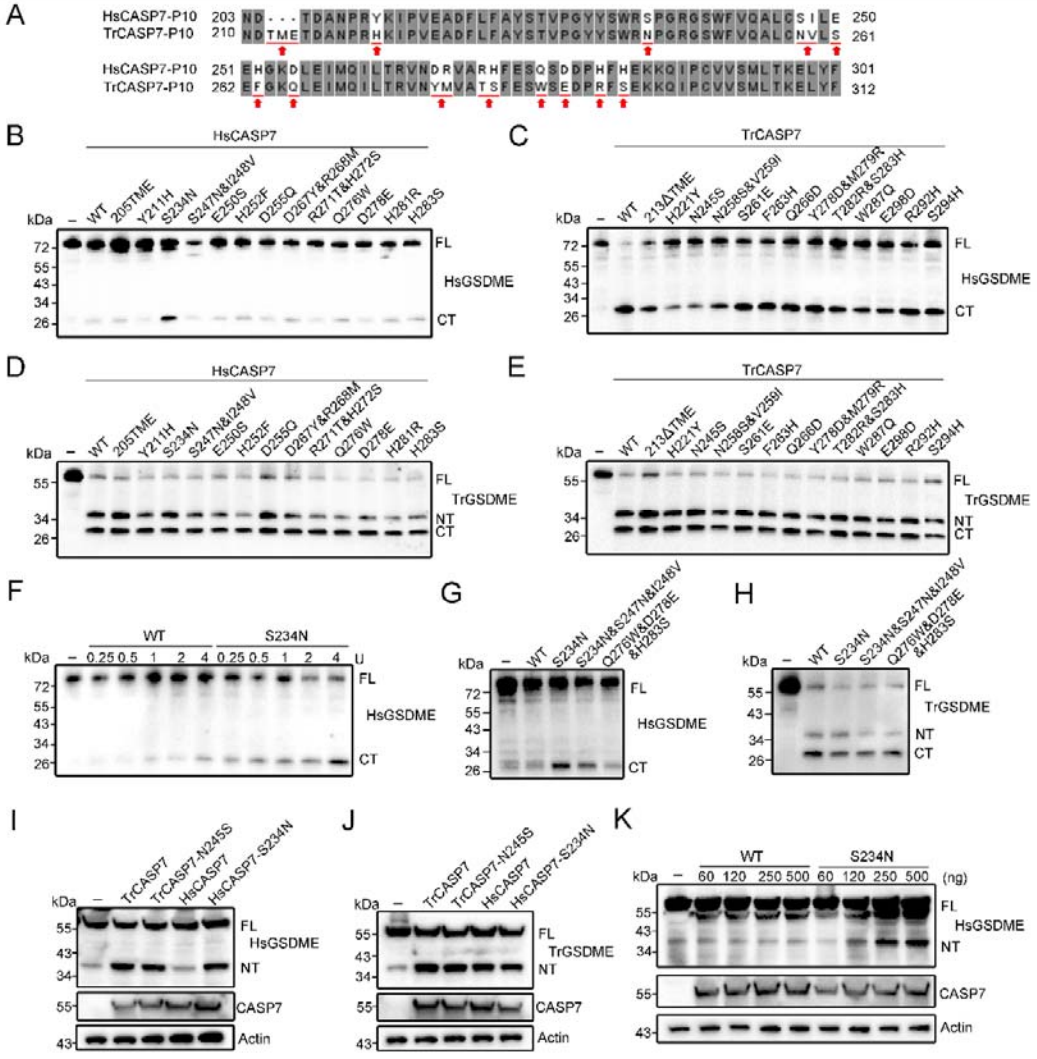
A
HsCASP7-P10 203 ND---TDANPRYKIPVEADFLFAYSTVPGYYSWRSPGRGSWFVQALCSILE 250
TrCASP7-P10 210 NDTME TDANPRHKIPVEADFLFAYSTVPGYYSWRNPGRGSWFVQALCNVLS 261
HsCASP7-P10 251 EHGKDLEIMQILTRVNDRVARHFESQSDDPHFHEKKQIPCVVSMLTKELYF 301
TrCASP7-P10 262 EFGKQLEIMQILTRVNYMVATSFESWSEDPRFSEKKQIPCVVSMLTKELYF 312
B
HsCASP7
WT 205TME Y211H S234N S247N&I248V E250S H252F D255Q D267Y&R268M R271T&H272S Q276W D278E H281R H283S
kDa
72
55
43
34
26
FL
HsGSDME
CT
C
TrCASP7
WT 213ΔTME H221Y N245S N258S&V259I S261E F263H Q266D Y278D&M279R T282R&S283H W287Q E298D R292H S294H
kDa
72
55
43
34
26
FL
HsGSDME
CT
D
HsCASP7
WT 205TME Y211H S234N S247N&I248V E250S H252F D255Q D267Y&R268M R271T&H272S Q276W D278E H281R H283S
kDa
55
34
26
FL
TrGSDME
NT
CT
E
TrCASP7
WT 213ΔTME H221Y N245S N258S&V259I S261E F263H Q266D Y278D&M279R T282R&S283H W287Q E298D R292H S294H
kDa
55
34
26
FL
TrGSDME
NT
CT
F
WT
S234N
kDa – 0.25 0.5 1 2 4 0.25 0.5 1 2 4 U
72
55
43
34
26
FL
HsGSDME
CT
G
WT S234N S234N&S247N&I248V Q276W&D278E &H283S
kDa
72
55
43
34
26
FL
HsGSDME
CT
H
WT S234N S234N&S247N&I248V Q276W&D278E &H283S
kDa
55
43
34
26
FL
TrGSDME
NT
CT
I
TrCASP7 TrCASP7-N245S HsCASP7 HsCASP7-S234N
kDa
55
43
34
FL
HsGSDME
NT
55
CASP7
43
Actin
J
TrCASP7 TrCASP7-N245S HsCASP7 HsCASP7-S234N
kDa
55
43
34
FL
TrGSDME
NT
55
CASP7
43
Actin
K
WT
S234N
kDa 60 120 250 500 60 120 250 500 (ng)
55
43
34
FL
HsGSDME
NT
55
CASP7
43
Actin

Figure 6

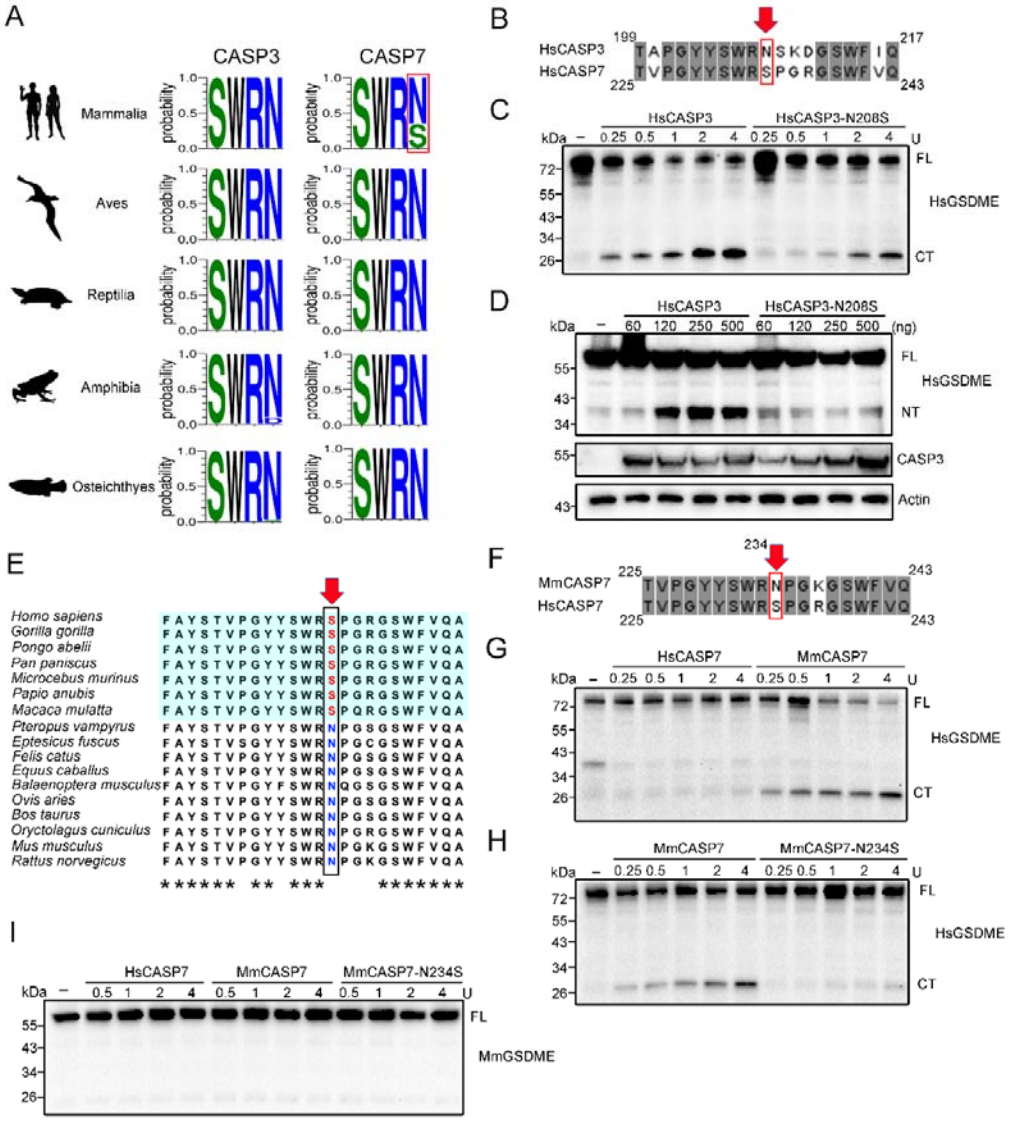
A
CASP3
CASP7
Mammalia
Aves
Reptilia
Amphibia
Osteichthyes
probability
B
HsCASP3
HsCASP7
199
217
225
243
C
HsCASP3
HsCASP3-N208S
kDa
0.25 0.5 1 2 4 0.25 0.5 1 2 4 U
72
55
43
34
26
FL
CT
HsGSDME
D
HsCASP3
HsCASP3-N208S
60 120 250 500 60 120 250 500 (ng)
55
43
34
FL
NT
HsGSDME
CASP3
Actin
E
Homo sapiens
Gorilla gorilla
Pongo abelii
Pan paniscus
Microcebus murinus
Papio anubis
Macaca mulatta
Pteropus vampyrus
Eptesicus fuscus
Felis catus
Equus caballus
Balaenoptera musculus
Ovis aries
Bos taurus
Oryctolagus cuniculus
Mus musculus
Rattus norvegicus
F
MmCASP7
HsCASP7
234
225
243
G
HsCASP7
MmCASP7
0.25 0.5 1 2 4 0.25 0.5 1 2 4 U
FL
CT
HsGSDME
H
MmCASP7
MmCASP7-N234S
FL
CT
HsGSDME
I
HsCASP7
MmCASP7
MmCASP7-N234S
0.5 1 2 4 0.5 1 2 4 0.5 1 2 4 U
55
43
34
26
FL
MmGSDME

Figure 1-figure supplement 1

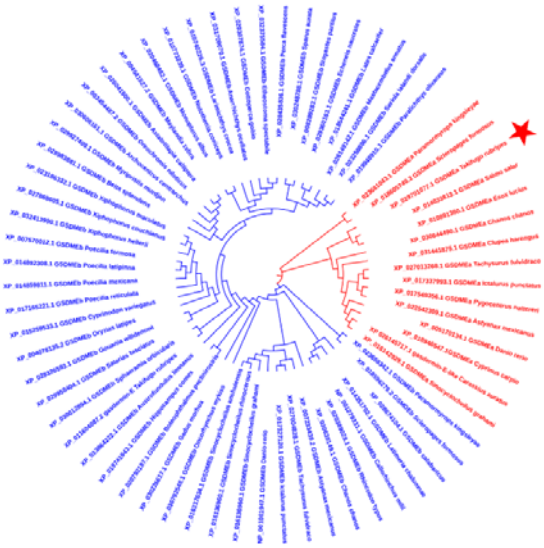

Figure 1-figure supplement 2

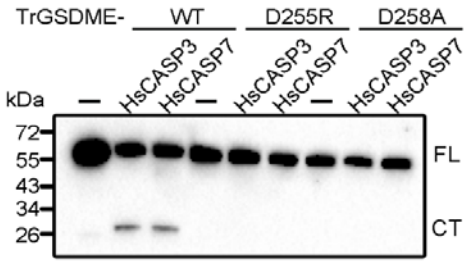

Figure 2-figure supplement 1

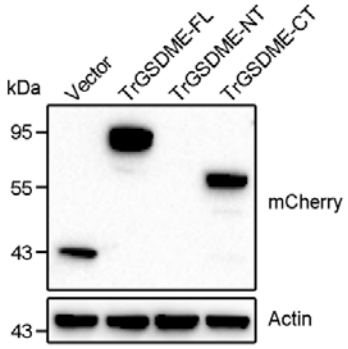

Figure 2-figure supplement 2

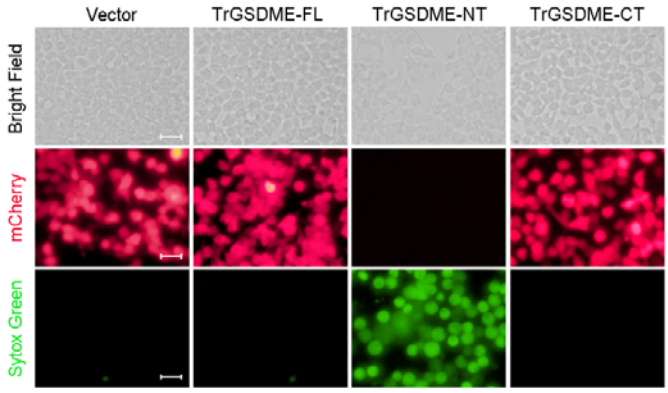

Figure 2-figure supplement 3

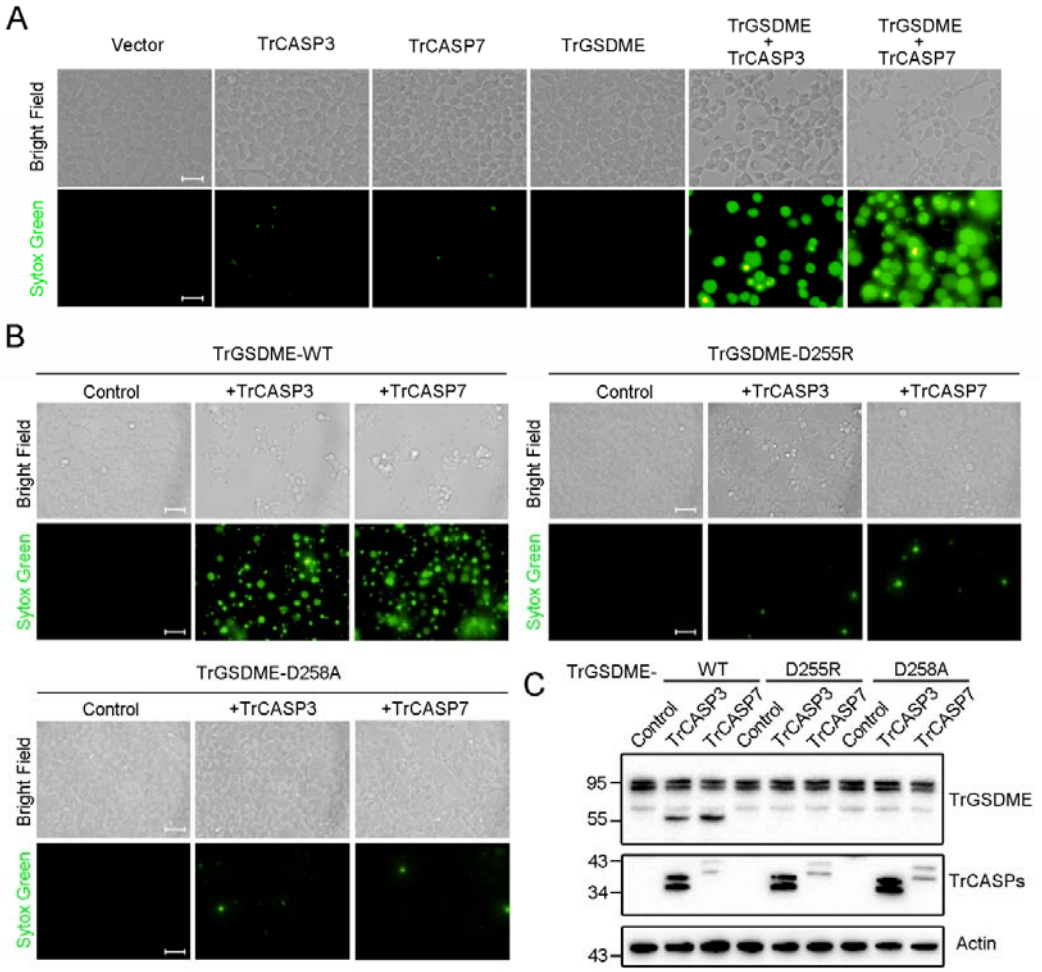

Figure 3-figure supplement 1

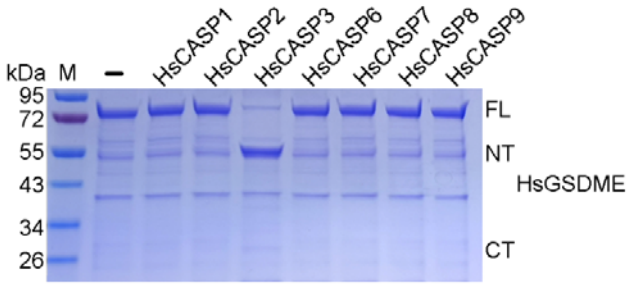

Figure 3-figure supplement 2

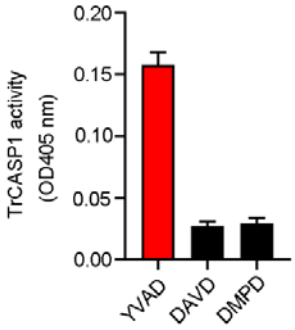

Figure 4-figure supplement 1

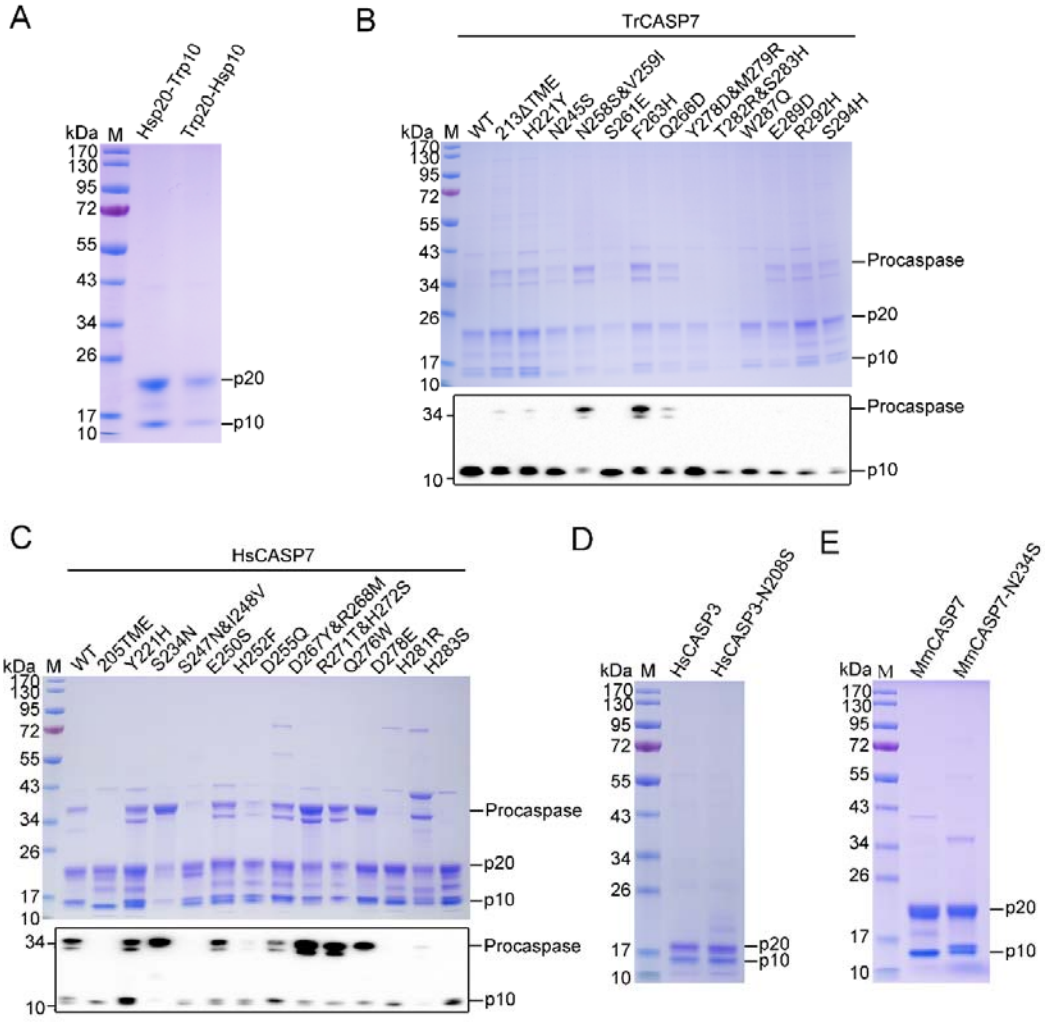

Figure 5-figure supplement 1

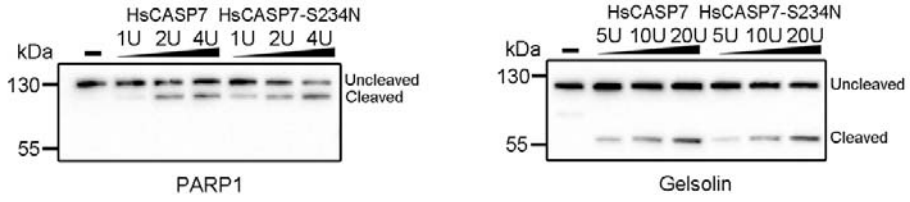

Figure 5-figure supplement 2

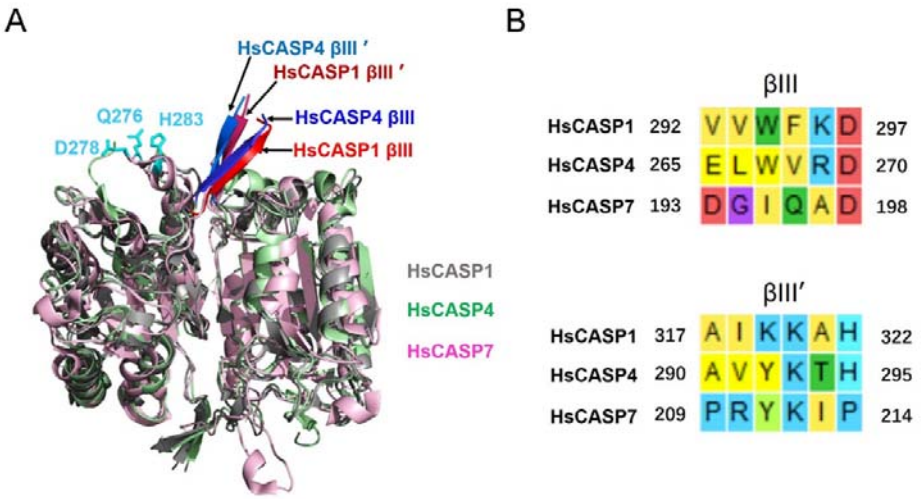

Figure 5-figure supplement 3

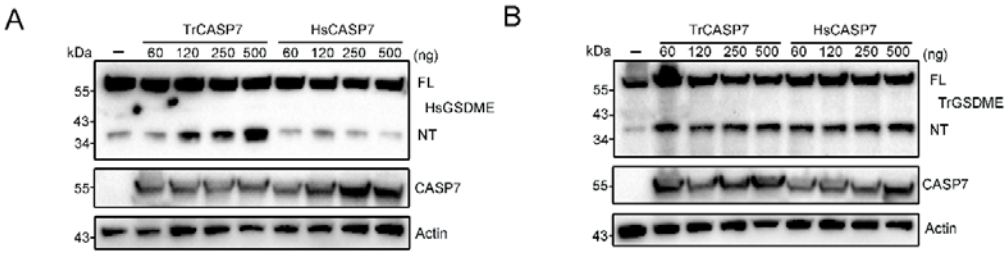

Figure 6-figure supplement 1

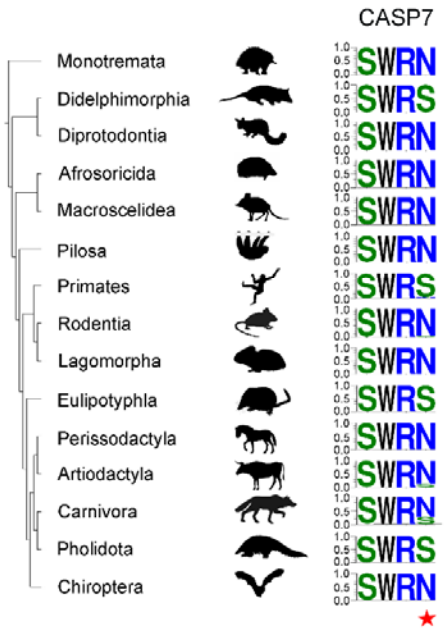

Figure 6-figure supplement 2